

RADC-TR-77-216 Interim Technical Report June 1977



INVESTIGATION OF ARRAY TECHNIQUES FOR MULTIPLE BEAMS WITHIN LIMITED SPATIAL SECTORS

Ground Systems Group Hughes Aircraft Company

Approved for public release; distribution unlimited



FILE COPY

ROME AIR DEVELOPMENT CENTER AIR FORCE SYSTEMS COMMAND GRIFFISS AIR FORCE BASE, NEW YORK 13441

This report has been reviewed by the RADC Information Office (01) and is releasable to the National Technical Information Service (NTIS). At NTIS it will be releasable to the general public, including foreign nations.

This technical report has been reviewed and approved for publication.

APPROVED: Richt Printlong ROBERT J. MAILLOUX Project Engineer

APPROVED:

ALLAN C. SCHELL

Acting Chief

Electromagnetic Sciences Division

FOR THE COMMANDER: Jahn J. Cucs

Plans Office

Unclassified

SECURITY OLDSSIFICATION OF THIS PAGE (When Data Entered) READ INSTRUCTIONS
BEFORE COMPLETING FORM / REPORT DOCUMENTATION PAGE 2 GOVT ACCESSION NO. 3 RADC-TR-77-216 TE ST REPORT & PERIOD COVERED 4. TITLE (and Subtitle) INVESTIGATION OF ARRAY TECHNIQUES FOR Scientific Report No-1 |_ MULTIPLE BEAMS WITHIN LIMITED SPATIAL SECTORS 5. PERFORMING ORG. REPORT NUMBER AUTHOR(s) CONTRACT OR GRANT NUMBER(s) R./Tang D.M.Joe F19628-75-C-0196 F. McNee. N.S. Wong 9. PERFORMING ORGANIZATION NAME AND ADDRESS TOCC AV FLEMENT, PROJECT Hughes Aircraft Company / 62702F Post Office Box 3310 46001425 Fullerton, California 92634 11. CONTROLLING OFFICE NAME AND ADDRESS
Deputy for Electronic Technology (RADC) 12. REPORT DATE June 1977 Hanscom AFB, Massachusetts 01731 NUMBER OF PAGES Monitor/Robert J. Mailloux/ETER SECURITY CLASS. (of this report) 14. MONITORING AGENCY NAME & ADDRESS(if different from Controlling Office Unclassified DECLASSIFICATION DOWNGRADING 16. DISTRIBUTION STATEMENT (of this Report) Approved for public release; distribution unlimited. 17. DISTRIBUTION STATEMENT (of the abstract entered in Block 20, if different from Report) 18. SUPPLEMENTARY NOTES 19. KEY WORDS (Continue on reverse side if necessary and identify by block number) ARRAYS, MULTIPLE BEAMS, LIMITED SCAN, SUBARRAY, BEAM SWITCHING, OVERLAPPING, STACKED PILLBOX, BEAM FORMING MATRIX, BEAM COUPLING, BLOCK FEEDING 20. ABSTRACT (Continue on reverse side if necessary and identify by block number) An antenna technique which is capable of providing multiple independent beams over limited scan sections has been developed. This antenna design utilizes overlapping subarrays fed by a stacked-pillbox multiple beam lens. Beams generated by the multiple beam lens can be selected by a beam switching matrix. An antenna design has been worked out to provide 8 or 16 multiple simultaneous beams over an 8 degree half angle cone. The antenna depth is less than the aperture diameter so that it is compact. In this design, sidelobe level of -25 dB or lower is achieved with adjacent beams. DD FORM 1473 EDITION OF 1 NOV 65 IS OBSOLETE

172370

Unclassified
SECURITY CLASSIFICATION OF THIS PAGE (When Date Entered)

SECURITY CLASSIFICATION OF THIS PAGE(When Data Entered)

Across over at -2 dB. Multiple simultaneous beams with negligible beam coupling loss is accomplished by selecting beams which are more than one beam step apart.



UNCLASSIFIED

SECURITY CLASSIFICATION OF THIS PAGE(When Date Entered)

TABLE OF CONTENTS

| | | | Page | |
|------|--|---|------|--|
| I. | PROGRAM OBJECTIVES | | | |
| II. | OVERVIEW OF THE STUDY PROGRAM | | | |
| III. | ARRAY ELEMENT AND SUBARRAY PATTERN CONTROL | | | |
| | Α. | Principle of Operation of Overlapping Subarray | 3 | |
| | В. | Design of the Coupling Network | 5 | |
| | C. | Two Dimensional Overlapping Subarray Implementation | 9 | |
| | D. | Subarray Amplitude Distribution and Subarray Patterns | 11 | |
| IV. | MUL | TIPLE BEAMFORMING MATRIX (STACKED PILLBOXES) | 18 | |
| | Α. | Description of the Multiple Beamforming Matrix (Stacked Pillboxes) | 18 | |
| | В. | Phase Error Distribution and the Feed Scan Angle | 21 | |
| | C. | Aperture Distribution of the Pickup Array | 27 | |
| | D. | Beam Coupling Loss and Its Dependence on Crossover Level | 33 | |
| | Ε. | Method of Providing Amplitude Taper | 38 | |
| V. | ALTERNATE MULTIPLE BEAMFORMING MATRIX (CONSTRAINED LENS) | | | |
| | Α. | Description of the Multiple Beam Constrained Lens | 53 | |
| | В. | Optimal Selection of Lens Parameters | 57 | |
| | C. | Methods of Providing Sidelobe Control | 62 | |
| VI. | BEAM SWITCHING MATRIX | | | |
| | Α. | Description of the Beam Switching Matrix Design Without Block Feeding | 63 | |
| | В. | Beam Switching Matrix Design for Block Feeding | 66 | |
| | C. | Alternate Beam Switching Matrix Design for Block Feeding | 71 | |
| | D. | Typical Examples of Beam Switching Matrix | 73 | |
| | Ε. | Estimated Losses in the Beam Switching Matrix | 76 | |

TABLE OF CONTENTS (Continued)

| | | | Page |
|-------|---|---|------|
| VII. | SAMPLE MULTIPLE BEAM ANTENNA DESIGNS | | |
| VIII. | CON | CLUSIONS AND DISCUSSIONS | 90 |
| IX. | APPENDICES | | |
| | APPENDIX A | | |
| | 1. | Determination of Amplitude Weighting Coefficients and Definition of Feed Network to Meet Specific Requirements of Scan Coverage and Grating Lobe Suppression | 92 |
| | 2. | Grating Lobe Locations | 106 |
| | 3. | Numerical Results | 106 |
| | APPENDIX B – DETERMINATION OF TRANSMISSION COEFFICIENT BETWEEN ELEMENTS IN FEED ARRAY AND RECEIVE ARRAY | | |
| | 1. | Two-Dimensional Array | |
| | 2. | Linear Array | 113 |
| | APPENDIX C – ACTIVE ELEMENT PATTERN OF AN ELEMENT IN THE REGULARLY SPACED ARRAY | | |
| | APPE | NDIX D – BEAM SWITCHING MATRIX LOSSES | 118 |
| х. | REFI | ERENCES | 126 |

I. PROGRAM OBJECTIVES

The objective of the study program is to devise and investigate light-weight and compact antennas which are capable of forming multiple simultaneous independent beams within a limited spatial sector. Any one or more of these beams within the coverage sector should be accessible at any instant with good isolation between them. In addition, these multiple beam, limited scan antennas must meet the following specifications:

Beamwidth 1°

Scan Coverage Sector 8° half angle cone

Antenna Gain Drop-off due to Scanning <3 dB

Antenna System Losses minimum

Antenna Depth aperture diameter

In order to accomplish the above objective, the program has been divided into the following four tasks:

- 1. Array element and subarray pattern control.
- 2. Multiple beamforming network design.
- 3. Beam switching matrix study.
- 4. Comparative analysis of system complexity and performance.

II. OVERVIEW OF THE STUDY PROGRAM

Among the many antenna techniques which are capable of providing multiple beam-limited scan operation, the overlapping subarray in conjunction with a stacked-pillbox multiple beam lens has been demonstrated by extensive analysis that it can meet the design goals as delineated. It has the capability of grating lobe control by means of overlapping subarray pattern shaping. It has the flexibility of designing for a specified number of simultaneous independent beams so that the network complexity can be controlled for a limited number of these simultaneous beams. The use of stacked pillbox as multiple beamformer provides high beamforming efficiency, simplified multiple beam network design, and frequency-independent beam pointing for all multiple beams. This feature of frequency independence is very attractive for synchronous satellite to ground communication systems.

The sidelobe control of this multiple beam antenna has been investigated. The use of block feeding in the multiple beamforming matrix design has been demonstrated to be a very effective means of sidelobe control. The beam switching matrix design to provide a specified number of simultaneous beams has been investigated. The impact of block feeding on the beam switching matrix design has also been identified.

Typical overall designs have been worked out for systems with 8 or 16 simultaneous beams and certain restrictions on multiple beam independence.

III. ARRAY ELEMENT AND SUBARRAY PATTERN CONTROL

A. Principle of Operation of Overlapping Subarray

The basic principle of an overlapping subarray is illustrated in Figure III.1.b. For the purpose of comparison, a conventional subarray antenna approach is shown in Figure III.1.a. The overlapping subarray is similar to the conventional subarray in which a phase shifter is used to control the phase of a group of radiating elements within the antenna array. Each radiating element in the overlapping subarray is fed by the inputs from two or more subarrays instead of from one subarray as in the case of the conventional subarray antenna. In so doing, the overlapping subarray is very effective in controlling the subarray pattern shape to suppress the grating lobes in the array factor formed by the large spacing (several wavelengths) between the subarrays. In the example of Figure III.1.b, each subarray consists of ten elements. For a given subarray, the five branch lines of the right half of one subarray and the five branch lines of the left half of the adjacent subarray to the right are combined in a set of couplers before coupling into the radiating elements. In a similar manner, the five branch lines to the left half of the subarray are combined with the five branch lines of the right half of the subarray to the left. As a result, the subarray aperture size is twice as large as the subarray spacing and twice as large as the aperture size of the conventional subarray shown in Figure III.1.a. This overlapping causes the aperture illumination of each subarray to overlap with its two adjacent neighbors as shown in Figure III.1.b. In the example as shown in Figure III.1.b, a triangular illumination function for each subarray is assumed. A more general illumination function can be employed for an even more effective pattern control. The net sum of

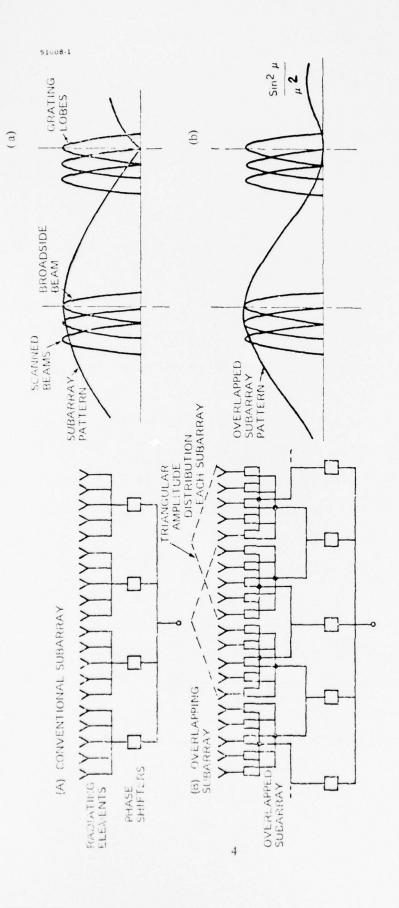


FIGURE III. I - BASIC PRINCIPLE OF AN OVERLAPPING SUBARRAY.

these superimposed illumination functions, when the input signals to the subarrays are inphase, yields a uniform illumination function across the array aperture as in the case of a conventional phased array. This is a necessary condition in order to achieve a lossless operation for the broadside beam. Since the illumination function for each subarray is triangular, the subarray pattern is $(\sin U/U)^2$ in form, where $U = kD \sin a$. The first null of this subarray pattern is located at the same angular position as that of the first grating lobe of the array factor since the aperture size of the subarray is twice as large as the subarray spacing. Furthermore, the subarray pattern does not rise steeply on either side of the null position since the slope of the subarray function is also zero at the null position, thus, allowing the suppression of the grating lobe over a wide angular scan coverage. The effectiveness of the overlapping subarray can be viewed from the standpoint of phase interpolation. When the array is scanned, the resultant phase at each element, due to the combined signals from two subarrays, assumes a value between the phase values of the two subarray phase shifters. If the relative amplitudes of the individual signals from the two phase shifters are selected properly in accordance to the element location within the subarray, the phase of the combined signal at the elements may assume a fairly linear function instead of the stepwise function of a conventional subarray antenna. This smoothing effect provides great benefit in suppression of grating lobes due to the large spacing between adjacent subarrays.

B. Design of the Coupling Network

The design of the coupling network at each element for a lossless operation is dependent upon the illumination function selected for each subarray. The selection of the illumination function is not completely arbitrary, only functions with the property indicated by the following formula would result in a

lossless operation for the broadside beam. This formula is given by:

$$A(x) + A\left(x - \frac{p}{2}\right) = constant$$

in which A(x) is the illumination function and p is the subarray aperture length. It is apparent that the triangular function satisfies the above condition. Other functions with the above characteristics include the cosine square on a pedestal. The best choice of the illumination function is dependent on the subarray size and the range of scan angles.

For the purpose of describing the design of the coupling network in detail, a sample case is shown in Figure III.2 in which three subarrays are shown: Subarrays A, B, and C. In general, for a given element in a subarray such as element d of Subarray A, the amplitude weighting coefficient may be denoted as A(x). Element d is also shared with Subarray B in which the amplitude weighting coefficient can be denoted as A(x-P). P is the subarray aperture length. The condition of the sum of the amplitudes being constant assures that the superimposed aperture distribution is uniform across the array corresponding to maximum broadside gain. The choice of the coupling coefficients for the power divider and the corporate feed is not arbitrary. They must be selected to meet the following conditions:

$$A(\mathbf{x}) + B(\mathbf{x}) = 2/N \tag{3-1}$$

$$|W_{g}(x)|^{2} + |W_{g}(x)|^{2} = 1$$
 (3-2)

in which

A(x) is the partial field at the radiating element caused by a unit wave at Subarray A.

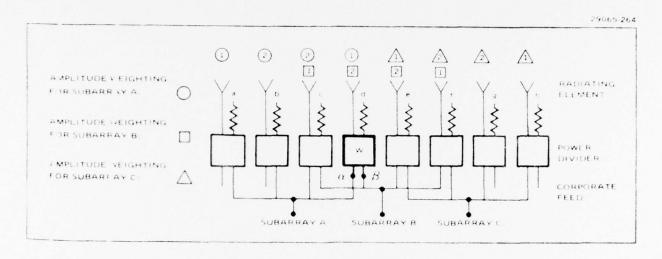


FIGURE III. 2 - COUPLING NETWORK IN THE OVERLAPPING SUBARRAY APPROACH.

B(x) is the partial field at the radiating element caused by a unit wave at Subarray B, and

 $\boldsymbol{W}_{\alpha}(\boldsymbol{x})$ and $\boldsymbol{W}_{\beta}(\boldsymbol{x})$ are coupling coefficients of the power divider.

Define the coupling coefficients of corporate feed for Subarray A as $\alpha(x)$ and for Subarray B as $\beta(x)$.

$$\begin{cases} A(\mathbf{x}) = \alpha(\mathbf{x}) \ W_{\alpha}(\mathbf{x}) \\ B(\mathbf{x}) = \beta(\mathbf{x}) \ W_{\beta}(\mathbf{x}) \end{cases}$$

Substituting these relationships into equation in Condition (3-1) gives the following:

$$\alpha(x) W_{\alpha}(x) + \beta(x) W_{\beta}(x) = \frac{2}{N}$$

Condition (3-2) can be satisfied if we let:

$$\begin{cases} \alpha(\mathbf{x}) = \frac{2}{N} W_{\alpha}^*(\mathbf{x}) \\ \beta(\mathbf{x}) = \frac{2}{N} W_{\beta}^*(\mathbf{x}) \end{cases}$$

Thus.

$$A(x) = \frac{2}{N} \left| W_{\alpha}(x) \right|^2$$

or,

$$|W_{\alpha}(x)| = \sqrt{\frac{N}{2}} A(x)$$

$$\alpha(x) = \sqrt{\frac{2}{N}} A(x)$$
(3-3)

$$C(\mathbf{x}) = \sqrt{\frac{2}{N}} A(\mathbf{x}) \tag{3-4}$$

Equations (3-3) and (3-4) give the coupling coefficients once the amplitude weighting coefficients are specified.

The above conditions assure a lossless operation for the broadside beam case; however, there will be losses in the coupling network when the beam is scanned away from broadside.

C. Two Dimensional Overlapping Subarray Implementation

The implementation of the overlapping subarray concept to meet the requirements of the multiple beam limited scan antenna as delineated previously is depicted in Figure III. 3. Linear overlapping subarrays are first formed in the manner as shown in Figure III.1.b. The inputs to these linear overlapping subarrays are then regarded as outputs of the overlapping subarrays in the orthogonal plane. Thus, each input terminal of the resultant two dimensional overlapping subarray transmits signals to 8 x 8 radiating elements in a square area, and the adjacent overlapping subarrays are spaced four elements apart. As a consequence, each radiating element may receive signals from four subarray inputs so that phase interpolation may be obtained in both principal planes. As shown, the number of subarrays is one-sixteenth of the total number of effective number of elements in the planar array. The design of a multiple beam matrix to process the signals at the subarray level is much simplified due to reduced number of channels. As shown in Figure III. 3, a two-dimensional Butler matrix is assumed to be the multiple beamforming network. Other multiple beamforming devices may prove more suitable. For example, the linear Butler matrices as shown in Figure III. 4 may be replaced by a circular pillbox if it is cumbersome to fabricate Butler matrix of excessive size. Another possibility may be the substitution of the entire two-dimensional Butler matrix by the HIHAT Iens or the multiple beam constrained Iens. Design of these

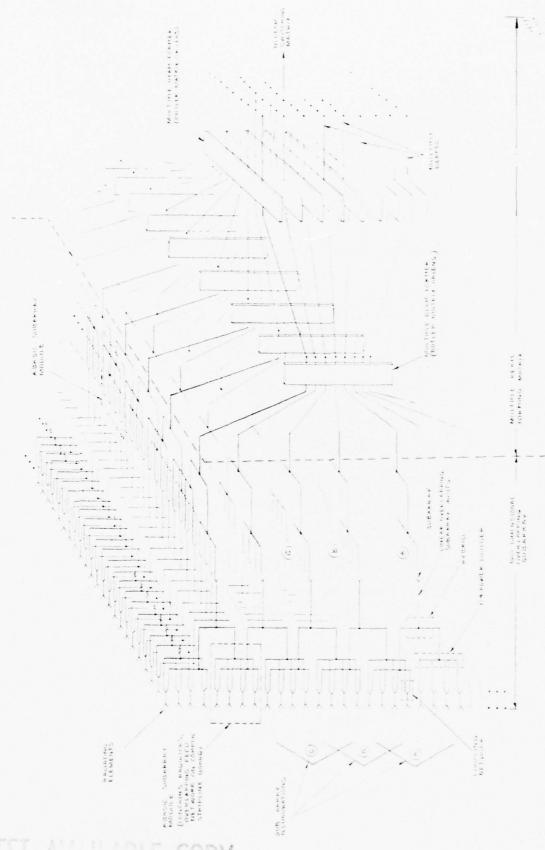


FIGURE III, 3 - TWO-DIMENSIONAL OVERLAPPING SUBARRAY WITH SIMULTANEOUS INDEPENDENT BEAMS.

lenses will be discussed in later sections. After these multiple beams are formed, a switching matrix may be used to select the beams. Methods of selection of any arbitrary set of beams has been worked out and will also be discussed further.

D. Subarray Amplitude Distribution and Subarray Patterns

The overlapping subarray with two levels of overlap as shown in Figure III.1.b has been designed for the present application. The weighting coefficients of the subarray can be selected to yield the best results on antenna gain and grating lobe suppression. The best compromise results when the grating lobes on both sides of the main beam are equalized at the scan limits. For grating lobe level on the order of -20 to -25 dB, the weighting coefficients of the subarray are given below:

Subarray Amplitude Distribution:

.1875, .400, .600, .8125, .8125, .600, .400, .1875

The far field subarray patterns are shown in Figure III.4 with element spacing as a parameter. The grating lobe regions for $\pm 8^{\circ}$ scan are also indicated in the figure. The first sidelobe of the array pattern can be lowered by a slight modification of the subarray amplitudes; therefore, the grating lobe level is governed by the drop-off of the main lobe of the subarray pattern as indicated by the cross hatched area in Figure III.4. The loss in gain and grating lobe level as derived from the subarray patterns are summarized in Figure III.5. It is quite clear that grating lobe levels of -20 to -25 dB are easily obtainable; however, the element spacing must be less than 2.1 λ in order to minimize the loss in gain at scan limits to less than 3 dB. It is possible to reduce the gain loss further by reducing the element spacing. For example, gain loss of 1.5 dB can be realized with element spacing of 1.5 λ , but the required number of subarrays

in each plane would increase by about 40 percent.

The network diagram of a three-level overlapping subarray is shown in Figure III.6. The determination of the subarray amplitude distributions and the network parameters for a given grating lobe level and gain reduction are discussed in detail in Appendix A. The far field subarray patterns for a near optimum set of subarray amplitudes are given in Figure III.7 for various element spacings. The loss in gain and grating lobe level are summarized in Figure III.8. It is evident that the case of a three-level overlap improves the loss in gain substantially, but the grating lobe suppression is significantly reduced. For example, a grating lobe of about -13 dB is obtained for element spacing of 2.1 λ (2.56 inches), and gain loss is only 0.5 dB. If a grating lobe level of -20 dB is required, the element spacing must be reduced to about 1.6 λ which increases the number of subarrays by 32 percent. These results indicate that two-level overlap can provide better sidelobe control at the expense of some gain loss, but the three-level overlap can provide good gain characteristics at some sacrifice of sidelobe level.

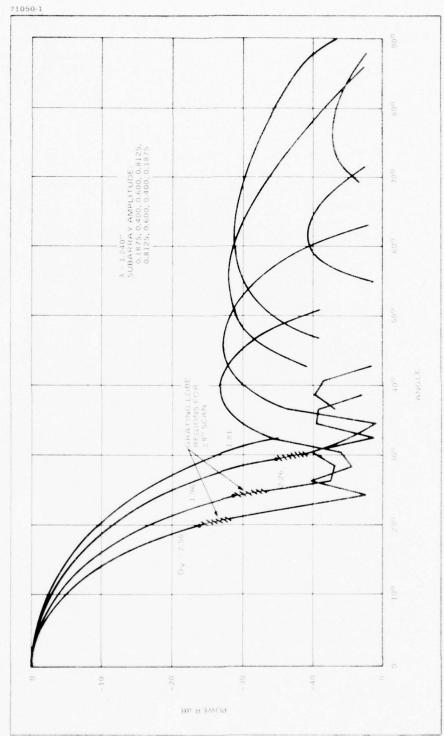


Figure III.4. Subarray Patterns of Overlapping Subarray, Two Levels of Overlap

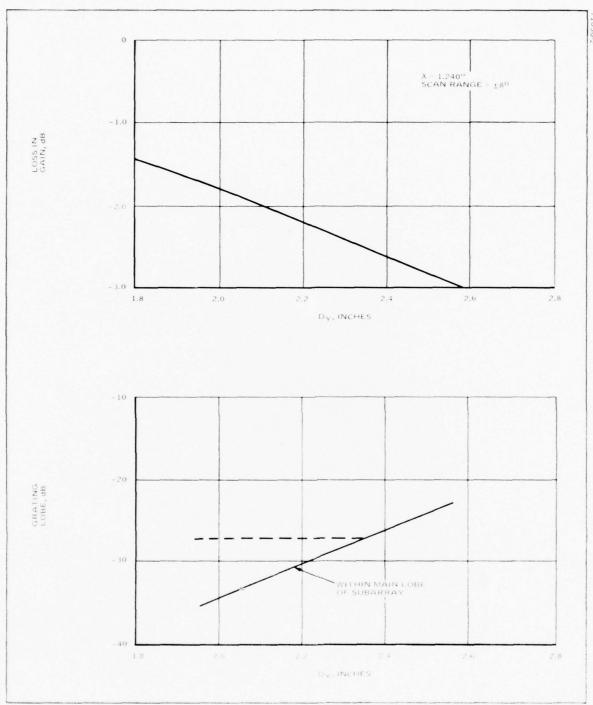
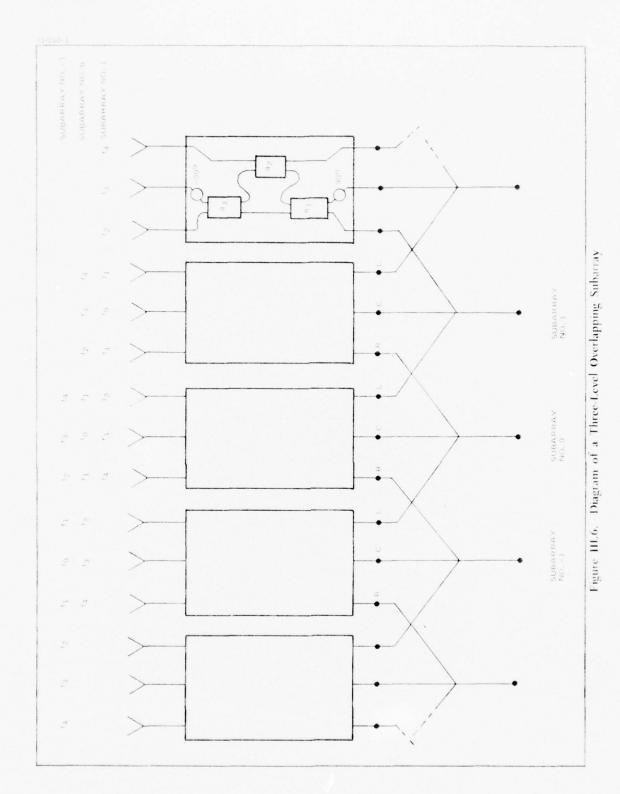


Figure III.5. Variation of Maximum Loss in Gain and Grating Lobe with Element Spacing (Two-Level of Overlap)



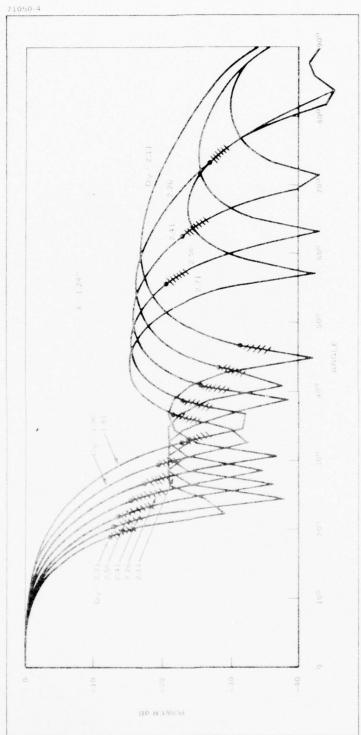


Figure 111.7. Subarray Patterns of Generalized Overlapping Subarray (Effect of Spacing on Grating Lobe Suppression)

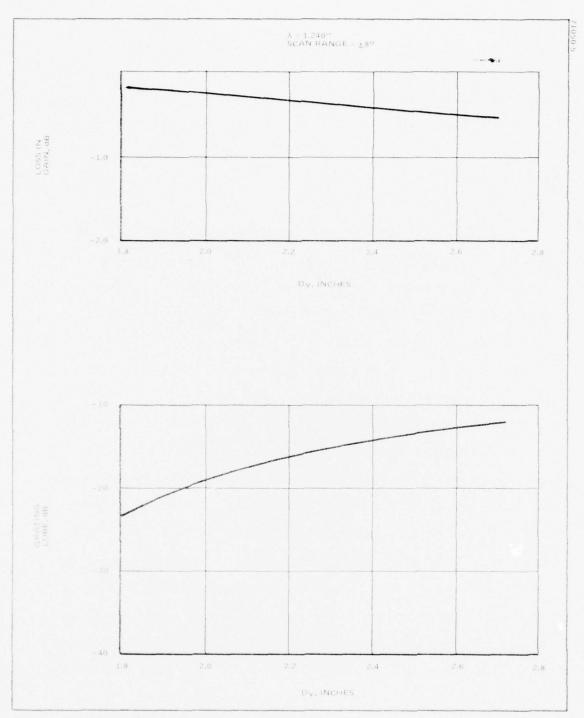


Figure III.8. Variation of Gain Loss and Grating Lobe Level With Element Spacing

IV. MULTIPLE BEAMFORMING MATRIX (STACKED PILLBOXES)

A. Description of the Multiple Beamforming Matrix (Stacked Pillboxes)

Application of the stacked pillboxes as a multiple beamforming matrix is illustrated in Figure IV.1. The multiple beamforming unit is comprised of two sets of circular pillboxes which are identified as the column lenses and the row lenses in the figure. Construction of each one of these pillboxes is shown in Figure IV.2. Each pillbox provides a quasi-linear phase front at the output terminals when a given feed array element is energized; thus, each feed array element to the row lenses as shown in Figure IV.1 generates a quasi-plane phase front at the output terminals at the column lenses. The outputs of the column lenses are connected to the N x N overlapping subarrays, which are arranged in a square lattice. Since every input terminal to the row lenses excites all overlapping subarrays with various progressive phase distribution, each input terminal is in fact a multiple beam input terminal of the multiple beamforming matrix. The number of input terminals of the row lenses is M x M, which corresponds to the number of beam positions within the desired coverage sector.

The circular pillbox is shown in Figure IV.2. Rotman² has described the operation of this device previously. Essentially, a feed horn illuminates a circular reflector and the reflected wave is received at the pick-up aperture. The phase distribution at the aperture is linear superimposed by a spherical aberration component. The circular reflector is folded to avoid feed blockage. The parallel plate region between the circular reflector and the pick-up aperture is folded once more to reduce the depth of the device and to locate the feed array and the pick-up array at opposite sides with respect to each other. The slope of the linear progressive phase distribution of each feed horn is dependent on the position of the feed horn in the feed array. As shown in Figure IV.2, the

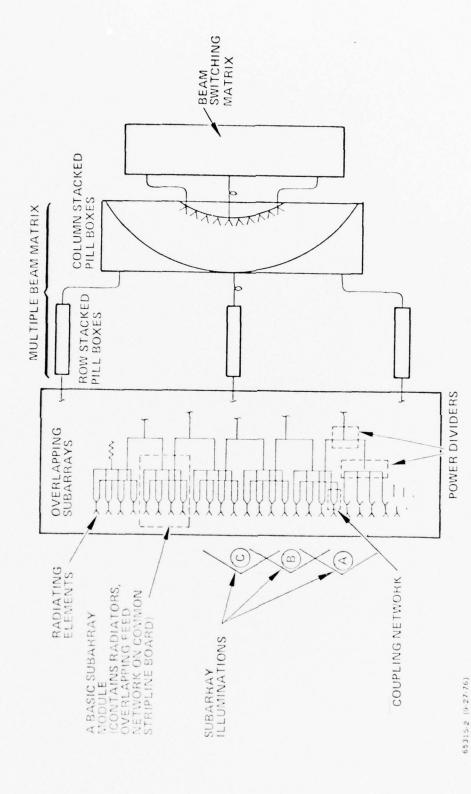


FIGURE IV, 1 - THE MULTIPLE BEAM FORMING MATRIX (STACKED PILLBOXES).

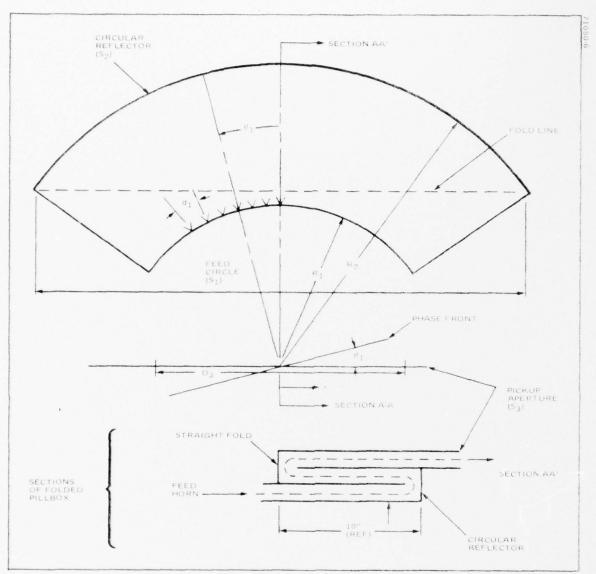


Figure IV.2. Circular Pillbox

feed horn, which is located at polar angle, θ_1 , from the center of the feed array forms a linear phase front at the pick-up aperture with angle θ_1 . Because of circular symmetry the shape of the phase error distribution due to spherical aberration for all feed horns is similar. By appropriate selection of the design parameters of the pillbox, the magnitude of the phase error can be controlled. Design parameters of significance include the following:

Radius of circular reflector, R₂

Radius of feed array, R1

Width of the pick-up aperture, D_3

Since the beam pointing angle of the pick-up aperture is dependent on the location of the feed horn, the spacing between the adjacent feed horns governs the separation between adjacent beam positions.

B. Phase Error Distribution and the Feed Scan Angle

The amplitude and phase distribution of the multiple beamforming matrix can be determined by tracing the signal flow through the network. Since all column and row lenses are identical, the distribution is a separable function of two variables; one term is given by the column lens and the other term is given by the row lens.

The far field pattern as derived from this weighting function is also separable in two principal planes. Consequently, the phase error from the row lens affects the azimuth plane patterns; whereas the phase error from the column lens affects the elevation plane patterns. For our present application, the row lens and column lens are identical to each other so that the phase error effect can be studied by calculating the phase error distribution on only one of the lenses.

The phase error distributions on each column or row lens (circular pillbox) have been calculated by the method of ray tracing. The results are shown in the family of curves in Figure IV.3. If we consider the useful portion of the aperture as bounded by the points in which the phase error curve crosses the axis, this aperture ratio, $D_3/(2R_2)$, can be determined as a function of R_2 for a specified allowable phase error such as $10^{\rm o}$ or $20^{\rm o}$. This relationship is plotted in Figure IV.4.a. Figure IV.4.b gives the ratio of R_1/R_2 for optimum adjustment of the feed focusing to minimize phase errors. It can be seen in Figure IV.4.a that a wider range of value of D_3 and R_2 can be chosen while the spherical aberration effect is fairly small. For example, a possible set of design parameters for phase error of $10^{\rm o}$ is listed below:

Maximum phase error within aperture (δ) = 10°

Radius of circular reflector (R₂) = 10λ

Width of pickup aperture (D₃) = 9.1λ

Radius of feed array (R₁) = 5.275λ

The aperture width of the phased array is in the area of 50 to 65λ ; therefore, the size of the pillbox as given by the above set of parameters is rather small when compared to the aperture size of the phased array.

As shown in Figure IV.3, phase error distribution on the pickup aperture varies with respect to the feed horn location or the beam position even though the shape of the error curve remains the same. If the phase error distribution does not vary a great deal for all beam positions of interest, a Schmidt type of correction may be applied to reduce the phase errors. Let's define the angle of normal to the plane wave at the pickup aperture as the feed scan angle θ_1 . This angle is identical to the horn location angle as mentioned previously. This angle θ_1 is related to the scan angle of the phased array in

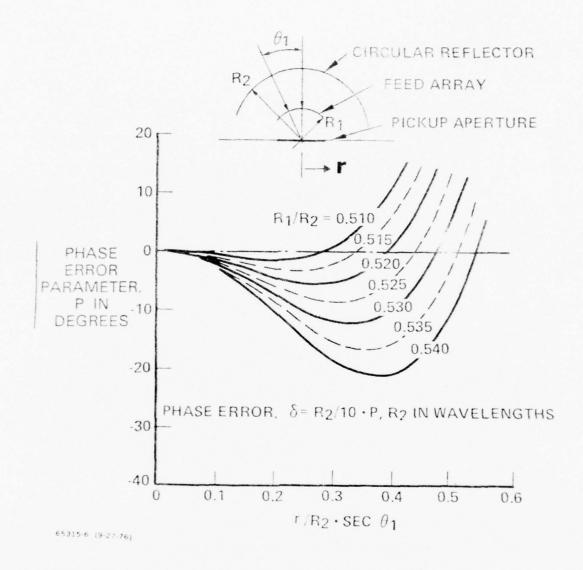


FIGURE IV. 3 - PHASE ERROR AT PICKUP APERTURE (BEFORE COMPENSATION)

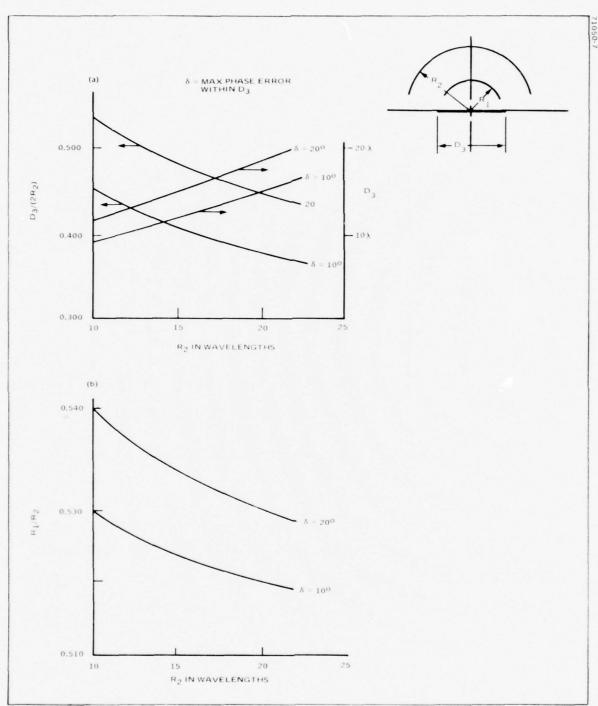


Figure IV.4. Selection of Design Parameters to Meet Specified Allowable Phase Error (Before Compensation)

the following manner:

$$\sin \theta_1 = \frac{D_4}{D_3} \sin \theta_2 \tag{4-1}$$

in which

 ${\rm D}_4$ is the aperture width of the phased array, and ${\rm H}_2$ is the scan angle of the phased array.

For the possible set of design parameters as mentioned, the feed angle exceeds $80^{\rm O}$, therefore, phase error control does not impose the lower limit on the size of the pillbox in this case. The dependence of the feed scan angle on the width of the pickup array is shown in Figures IV.5.a and IV.5.b. The first case is a $1^{\rm O}$ beam phased array with almost uniform amplitude weighting, and the second case is a $1^{\rm O}$ beam phased array with 30 dB Taylor weighting. If it is desired to maintain feed scan angle at $30^{\rm O}$ or less, the width of the pickup aperture is 14λ and 17λ for these two cases, respectively. The reasons for maintaining a small feed scan angle will be discussed further later on.

A possible set of design parameters for maximum feed scan angle of 30° is listed below:

Maximum feed scan angle, $\theta_1 = 30^{\circ}$

Amplitude taper on phased array = 30 dB Taylor

Width of phased array, $D_4 = 62\lambda$ (for 1° beam)

Width of pickup array, $D_3 = 17.5\lambda$ (see Figure IV.5.b)

Phase error before correction, $\delta_0 = 20^{\circ}$ (see Figure IV.5.a)

Radius of circular reflector, $R_2 = 20\lambda$ (see Figure IV.4.a)

Radius of feed array, $R_1 = 10.5\lambda$ (see Figure IV.4.b)

It is possible to reduce the phase error by a Schmidt type of correction at the pickup array. This error correction method requires insertion of line

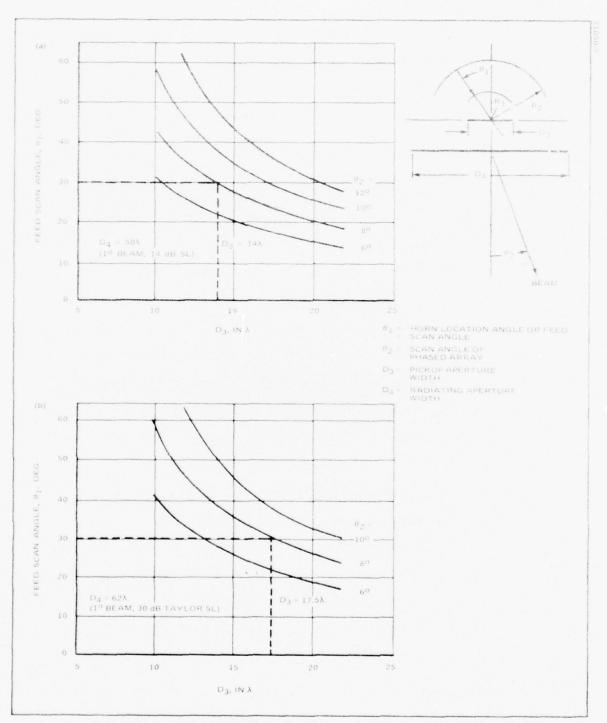


Figure IV.5. Dependence of Feed Scan Angle on Width of Pickup Array

lengths equal to the negative of the average equivalent line length due to the phase errors. This correction procedure has been carried out for the above design. The phase error distributions before correction and after correction are shown in Figures IV.6.a and IV.6.b, respectively. It is quite clear from observation of the two error distributions that phase error over much of the aperture is greatly improved, and the maximum phase error after correction is less than half of the maximum phase error before correction. Thus, this method of error correction is very effective and should be incorporated into the circular pillbox design. In this case, the maximum phase error after correction is only 8° which should permit realization of our sidelobe objective of 20-25 dB.

C. Aperture Distribution of the Pickup Array

1. Analysis

The calculation is for the transmit mode of operation, and unity power is incident on feed horn A as shown in Figure IV.7. The calculation is performed in two steps: (a) field at reflector due to feed array, (b) field at pickup array due to field on reflector.

(a) Computation of Field on Reflector

The reflector is divided into small segments of length ${\bf d}_2.$ The power received by any of these segments is given by:

$$P_2 = g_{12}^2 P_i$$

in which $\mathbf{P_i}$ is the incident power on feed horn, and is equal to 1.

 $\ensuremath{\mathbf{g}}_2$ is the transmission coefficient from feed horn to a small segment of reflector.

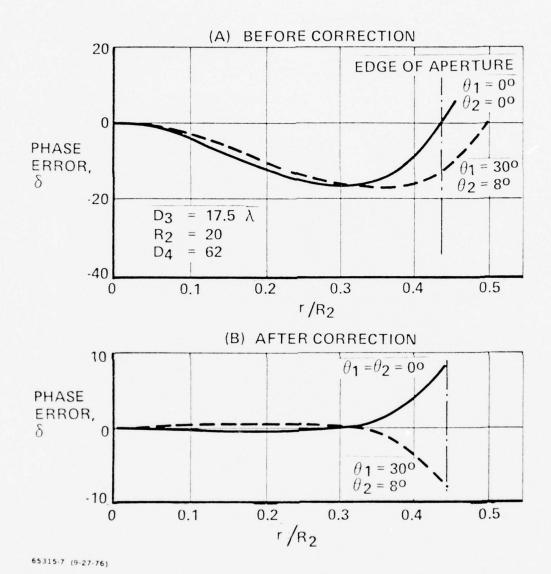


FIGURE IV.6 - PHASE ERROR DISTRIBUTION AFTER SCHMIDT CORRECTION.

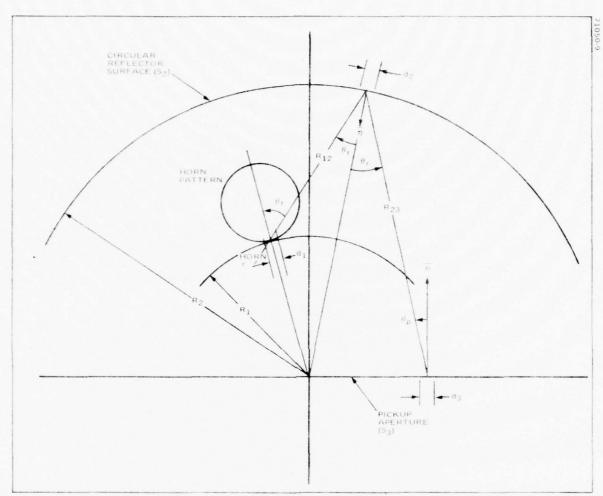


Figure IV.7. Circular Pillbox Geometry for Analysis of Aperture Field

The determination of transmission coefficient is shown in Appendix B (equation B-12). It is given below:

$$g_{12}^2 = \frac{d_1 d_2}{R_{12} \lambda} S_i^2(\theta_f) S_2^2(\theta_r)$$
 (4-2)

in which

d, is feed element spacing

 $\boldsymbol{\mathsf{d}}_2$ is spacing of sample points on reflector

 $\mathrm{S}_{1}^{2}(\boldsymbol{\theta}_{f})$ is active power element pattern of feed horn

 $s_2^2(\theta_r)$ is active power element pattern of a segment of reflector and is equal to $\cos\theta_r$, and R_{12} is the distance between feed horn and the reflector 1.

The field on the reflector is given by:

$$\begin{split} \mathbf{E}_{\text{ref}} &= \sqrt{P_{2}} \ \mathbf{e}^{-\mathrm{j}2 \pi R} \mathbf{12} \\ \\ \mathbf{E}_{\text{ref}} &= \sqrt{\frac{d_{1} d_{2}}{R_{12} \lambda}} \ \mathbf{S}_{1}(\theta_{\mathrm{f}}) \ \mathbf{S}_{2}(\theta_{\mathrm{r}}) \ \mathbf{e}^{-\mathrm{j}2 \pi R} \mathbf{12} \end{split} \tag{4-3}$$

(b) Computation of field on aperture of pickup array.

In this case, the contribution from each segment of the reflector is computed and then summed to obtain the total field at the aperture. Following the same procedure as part (a), the field at any element in the pickup array is given as:

$$E_{p} = \sum_{\substack{\text{all} \\ \text{segments}}} E_{\text{ref}} \sqrt{\frac{d_{2}d_{3}}{R_{23}\lambda}} S_{2}(\theta_{r}) S_{3}(\theta_{p}) e^{-j2\pi R_{23}}$$

$$(4-4)$$

in which

 E_p is the wave amplitude at the pickup array element d_3 is the element spacing of the pickup array $S_3(\theta_p)$ is the active amplitude element pattern of the pickup array, and

 \mathbf{R}_{23} is the distance between the pickup array and the reflector.

The active element patterns $S_2(\frac{\theta}{r})$ and $S_3(\frac{\theta}{p})$ can be represented by $\cos\theta_r$ and $\cos\theta_p$, respectively; however, the active element pattern of the feed horn $S_1(\theta_f)$ possesses more directive patterns than the cosine function because of the large spacing. An empirical formula has been developed for $S_1(\theta_f)$ in Appendix C. Essentially, it still assumes the cosine function over the scan range without grating lobes, and assumes faster rolloff outside this range.

2. Numerical Results of a Multiple Beam Overlapping Subarray
Antenna Design (Multiple Beamforming Matrix Comprised of
Stacked Pillboxes).

Based on the design data in Figures IV.3, IV.4, and IV.5, an antenna design has been worked out to yield I^o beamwidth and 3 dB crossover between beams. The circular pillbox for this antenna design is shown in Figure IV.8. The design parameters are indicated in the figure. For this design, the analytical formula as derived in the last section, was used to compute the aperture distributions on the pickup array. The amplitude

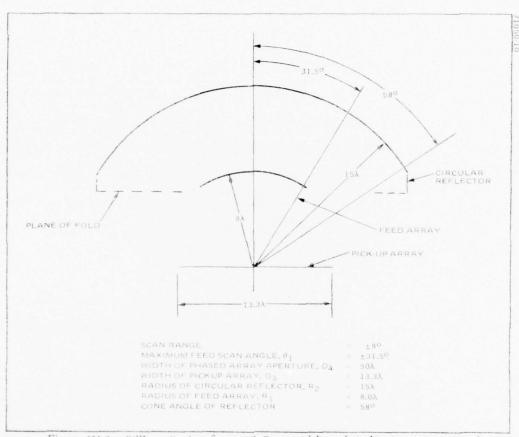


Figure IV.8. Pillbox Design for a 10 Beamwidth and 3 dB Cross Over Level

distributions as a function of scan are shown in Figure IV.9, and the phase distributions as a function of scan are shown in Figure IV. 10. The amplitude distribution is almost uniform for all scan angles; therefore, the close-in sidelobes are in the -14 dB level. Because the amplitude distribution rolls off sharply outside the pickup array aperture, the spillover and mutual coupling loss in each pillbox is only .57 dB. Because the multiple beamforming matrix consists of two sets of pillboxes in cascade, the combined loss for the multiple beamforming matrix is 1.14 dB. The spillover and mutual coupling loss can be identified as beam coupling loss as will be discussed further later on. Stein has computed the beam coupling loss of a multiple beam antenna in which uniform distribution is used for all beams. He computed a value of 1.25 dB $(q^2 = .75 \text{ in Figure 4 of Stein's paper})$ for crossover level of 3 dB between beams. The phase error across the aperture is very small which collaborates with the results obtained by ray tracing previously. The far field patterns were computed from the aperture distributions and are shown in Figure IV.11. In general, sidelobe level of -14 dB is obtained for all beams, which is expected for near optimum amplitude distributions.

D. Beam Coupling Loss and Its Dependence on Crossover Level

An excellent discussion of beam coupling in multiple beam antennas has been published by Stein. He defined the term, "radiation efficiency" as the fraction of power radiated from the feed. Radiation efficiency is denoted by q_k^2 , k being the index of the multiple beam. $1 - |q_k|^2$ represents the power loss between the input terminal to the kth beam. We may identify this term as

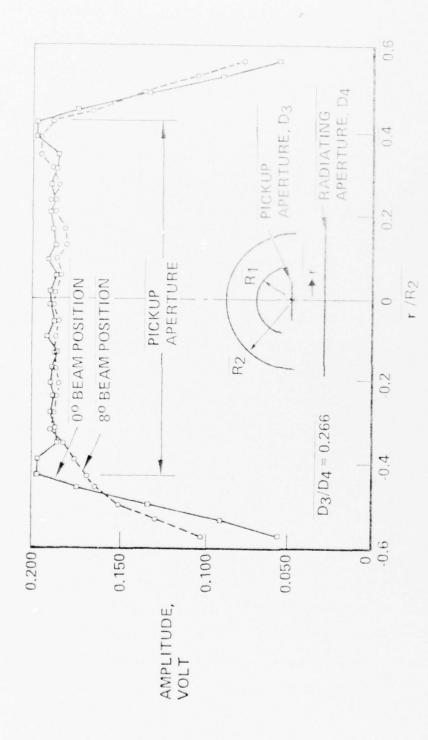


FIGURE IV, 9 - EXAMPLE AMPLITUDE DISTRIBUTIONS ON PICKUP APERTURE.

65315-8 (9-27-76)

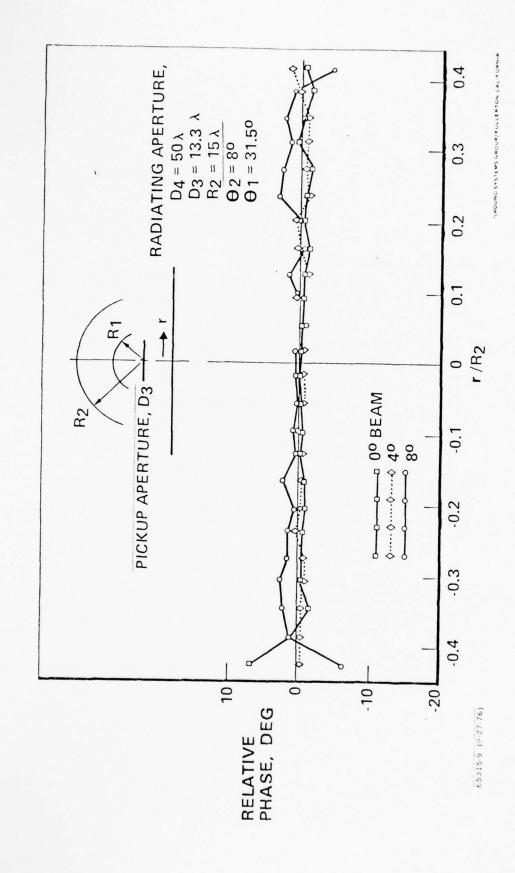


FIGURE IV. 10 - RESIDUAL PHASE ERROR AFTER A SCHMIDT CORRECTION.

"beam coupling loss," L_K. Thus, for unity input power at the feed horn, the radiated power from the antenna aperture is given as the portion of power contained within the illumination angle. The balance is accountable by power contained outside the illumination angle identifiable as "spillover loss" and coupling from the feed array element to other radiating elements within the array, which is identifiable as "mutual coupling loss." In the above viewpoint, beam coupling loss is the sum of spillover and mutual coupling losses for the stacked pillbox multiple beam antenna.

The power per unit arc length radiated by the feed horn into free space as distance R from the feed is $G(\theta)/(2\pi R)$. The total radiated power contained within illumination angle 2%, is

$$P_{r} - \int_{-\varpi}^{\varphi} \frac{1}{2\pi} G(\theta) d\theta = q^{2}$$
 (4-5)

 $G(\theta)$ is the gain function of the feed array element.

The gain function of feed array element is given as

$$G(\theta) = \frac{2\pi d_1}{\lambda} S^2(\theta)$$

The gain function and the active element pattern $S(\theta)$ are discussed in Appendix B and Appendix C, respectively. Substitute $G(\theta)$ into equation (4-6), we obtain the following:

$$q_2 = \int_{-\infty}^{\varphi} \frac{d_1}{\lambda} s^2(\theta) d\theta \tag{4-6}$$

The above equation is rather instructive. If we assume that the feed array element spacing has been selected so that d_1 and $S(\theta)$ are known, reducing the

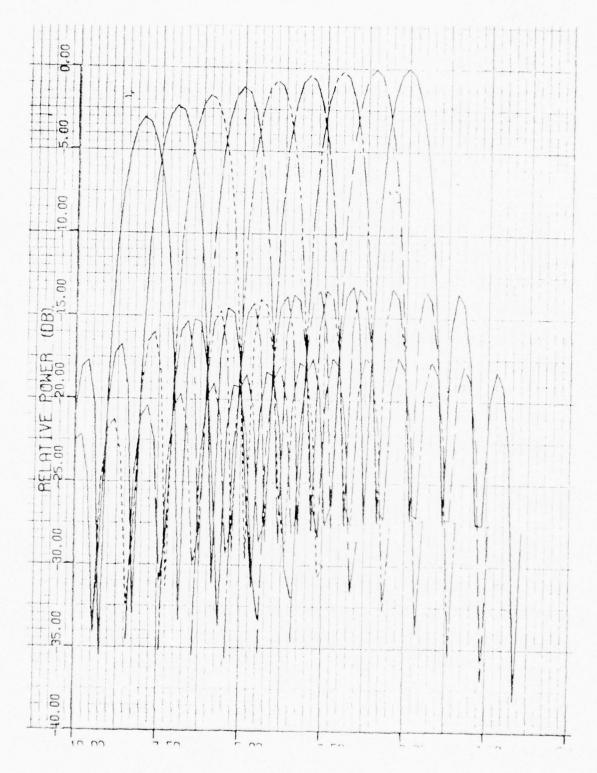


FIGURE IV. 11 - FAR FIELD PATTERN FOR DESIGN IN FIGURE IV. 8.

illumination half angle \circ would reduce the radiation efficiency q^2 . This observation is obvious from the standpoint of spillover loss as small illumination angle tends to increase the spillover loss of reflector antennas. The illumination angle is a monotonic function of $(D_3/2R_2)$; thus, increasing R_2 after the feed element spacing is fixed means increasing spillover loss and reduced radiation efficiency. By going through similar line of argument, it can also be concluded that increasing the feed element spacing d₁ after the circular reflector radius R₂ is fixed would tend to reduce spillover loss and increase radiation efficiency. For the design in the last section, the beam coupling loss was determined to be $1.14~\mathrm{dB}$ for a 1^o beamwidth antenna with 3 dB crossover between the adjacent beams. Designs in which other feed element spacing is used so that crossover level other than 3 dB is obtained have also been worked out. The beam separation of these designs is given in Figure IV.12.a. The beam coupling loss is given in Figure IV.12.b. The effect on beam coupling loss due to crossover level is summarized in Figure IV.12.c. It is rather remarkable that beam coupling loss depends principally on beam crossover, but not on feed element spacing of pickup aperture size.

E. Method of Providing Amplitude Taper

When the feed array element spacing and circular reflector radius were selected to yield a 2 to 4 dB crossover level between beams, the amplitude distribution for each beam was almost uniform. The associated sidelobe level is about 14 dB. It is obvious that a means to increase the amplitude taper is required to yield a sidelobe level in the order of 20 dB or below. Three methods are discussed below:

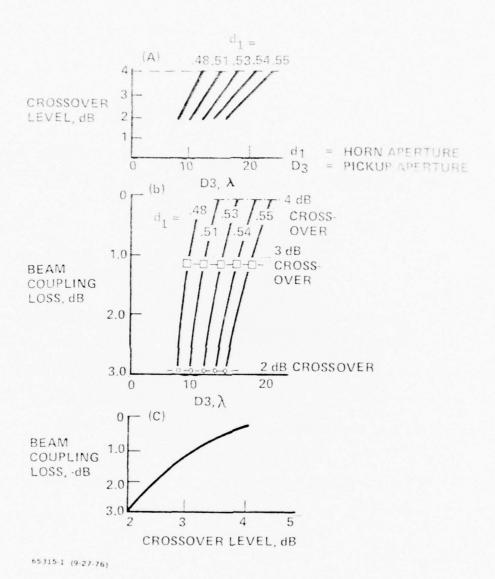


FIGURE IV.12 - BEAM COUPLING VERSUS CROSSOVER CHARACTERISTICS.

Resistive Tapering

The first method is to use attenuators at the outputs of the pickup aperture. Complete amplitude control is achieved with this method; however, the extra loss incurred is very high as shown by Table 4.1.

TABLE 4.1 – ADDITIONAL LOSS IN ANTENNA GAIN DUE TO RESISTIVE TAPERING

| Sidelobe Level (Taylor Distribution) | Resistive Loss for One Level of Pillbox | Additional Loss in Antenna Gain (2 Levels of Pillbox) | |
|---|--|---|--|
| 14 dB | 0 dB | 0 dB | |
| 20 | 2.1 | 4.2 | |
| 25 | 2.7 | 5.4 | |
| 30 | 3.1 | 6.2 | |

This additional loss is superimposed on the beam coupling loss as given in the above table. For 25 dB sidelobe design in both planes, and about 3 dB crossover level, the total beam coupling loss is 6.5 dB. The spillover and mutual coupling loss is 1.1 dB and the resistive tapering loss is 5.4 dB. Stein has computed the beam coupling loss for the $(1-r^2)$ distribution in which the first sidelobe is 24.6 dB. He obtained a beam coupling loss value of 3.2 dB for 3 dB crossover level. It is quite clear that resistive tapering is not an optimum method of achieving the desired sidelobe control.

Block Feeding

The second method is to use a block feeding technique in which two or more feed array elements are excited together. As shown previously, a typical feed array element produces nearly uniform distribution at the pickup aperture with a feed scan angle θ_1 . The adjacent element produces a similar amplitude

distribution and feed scan angle (θ_1 + S). S denotes the separation between adjacent beams. When these two elements are excited simultaneously, the resulting amplitude distribution is approximately a cosine function and the combined feed scan angle is (θ_1 + S/2). Figures IV.13 and IV.14 show two examples of the taper achieved by block feeding. In Figure IV.13, the beam separation before block feeding is equal to one beamwidth of the single element case. The edge taper in the amplitude distribution curve shown in Figure IV.13 is almost equal to the 30 dB Taylor distribution. The computed far field patterns shown in Figure IV.15 for this case indicate sidelobe levels of about -22 dB. Figure IV.14 shows the amplitude taper for the case with 1.23 beamwidths beam separation.

A stronger amplitude taper is produced in this case. The amplitude distribution curve is below the 30 dB Taylor distribution; however, the sidelobe level remains at about -22 dB because of the lack of precise control on the shape of the amplitude distribution.

Combination of Block Feeding and Resistive Tapering

The third method of amplitude control is to use a combination of block feeding and resistive tapering. Refer to Figures IV.13 and IV.14. The amplitude taper at the edges due to block feeding is quite adequate, yet low sidelobe levels are not produced because of the shape of the amplitude distribution. When these amplitude distributions are compared with the Taylor distributions, the difference between them is not great. Thus, it is permissible to trim the blockfed amplitude distributions by resistive tapering to produce a low sidelobe design without incurring large losses. The attenuator loss incurred in modifying the amplitude distribution in Figure IV.13 to a 30 dB Taylor is about 1.4 dB as compared to 6.2 dB when only resistive tapering is applied. In addition, the

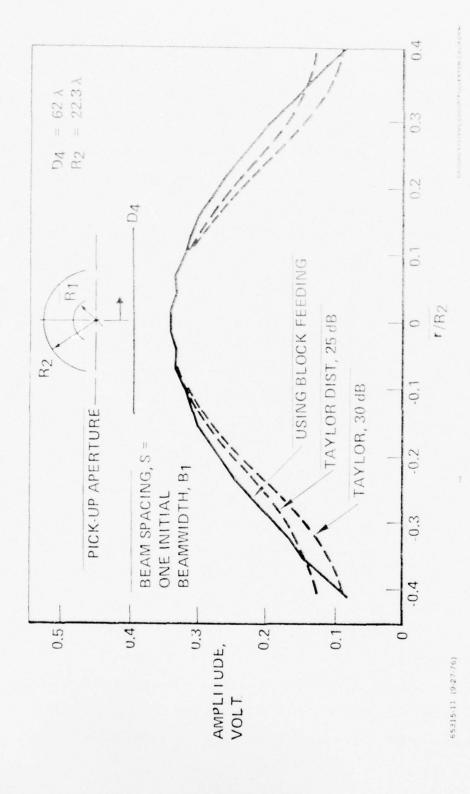


FIGURE IV, 13 - AMPLITUDE DISTRIBUTION USING BLOCK FEEDING.

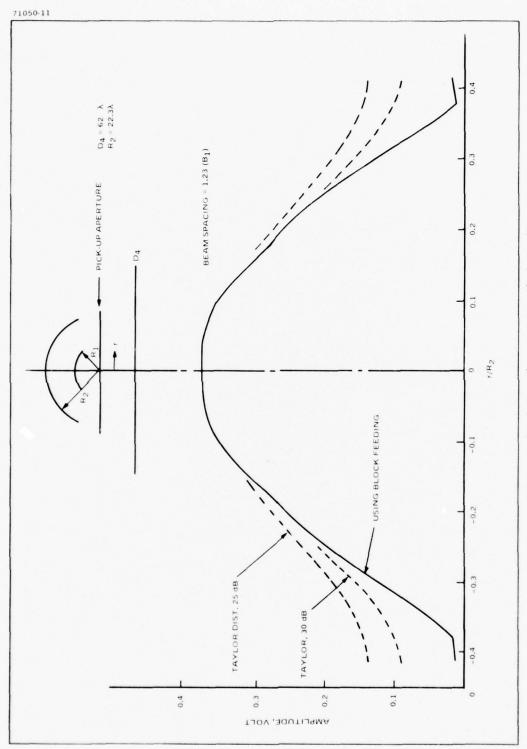


Figure IV.14. Amplitude Distribution Using Block Feeding

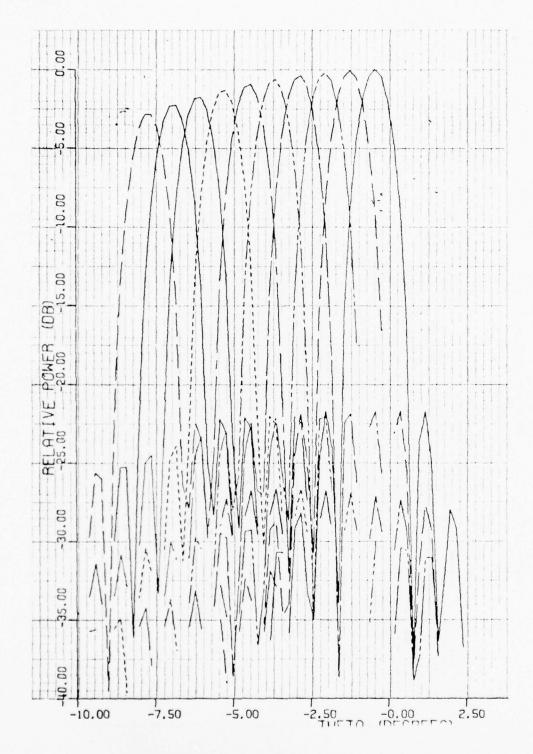


FIGURE IV. 15 - FAR FIELD PATTERN FOR BLOCK FEEDING OF TWO HORNS.

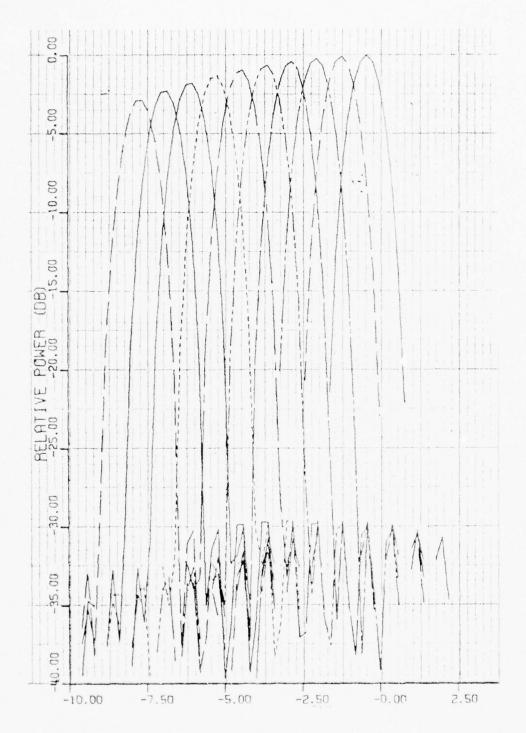


FIGURE IV.16 - FAR FIELD PATTERNS FOR BLOCK FEEDING OF TWO HORNS AND RESISTIVE TAPERING.

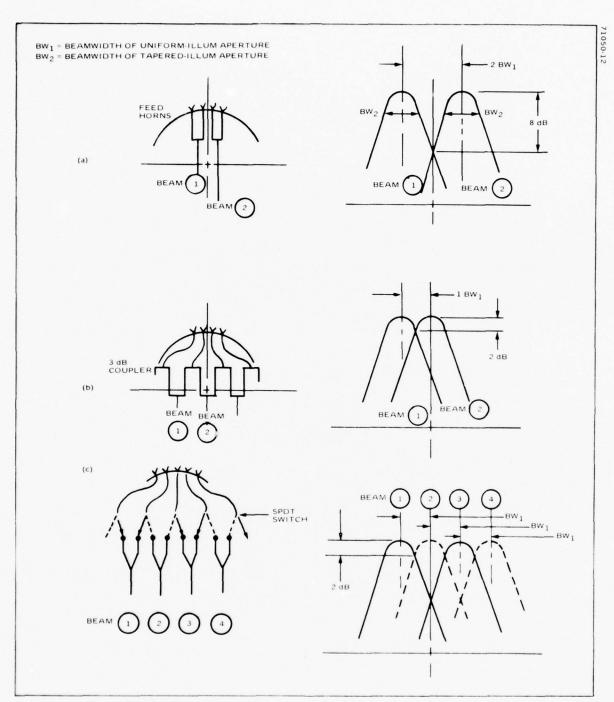


Figure IV.17. Beam Position Diagram with Block Feeding of Two Elements

loss component due to spillover and mutual coupling has also been virtually eliminated by block feeding. The far field patterns of this design have been computed and shown in Figure IV.16.

Crossover Level Between Beams when Block Feeding is Used

The beam crossover level and the beam coupling loss are dependent on the manner with which the feed element are fed and selected by the beam switching matrix. Figure IV.17 shows three possible ways of feeding. Beam selection in Figures IV.17.a and IV.17.b is identical to the case before block feeding is applied. Beam switching as indicated in Figure IV.17.c may be incorporated in the beam switching matrix; therefore, the beam switching matrix design for Figure IV.17.c is different from the first two cases. In Figure IV.17.a, adjacent horns are block-fed together by a magic-tee. Beam separation is given by the distance of two feed element spacings. The crossover level is 8 dB. Beam coupling loss is negligible because of the increase of directivity of the block-fed illumination pattern.

In Figure IV.17.b, each feed horn is connected to two beam ports through a 3 dB power divider. Beam separation is now given by one feed element spacing, and the crossover level rises to 2 dB. The beam coupling loss is 3 dB, which arises from the 3 dB power loss through the power divider.

In Figure IV.17.c, a feed horn may be switched to either one of the adjacent two-beam combining hybrids. In one switching position, beam I is generated. If one examines the switching operation in Figure IV.17.c closely, it is apparent that this switching position prevents the formation of beam 2. In general, selection of one beam prevents formation of the adjacent beams.

The crossover level between beams in Figure IV.17.c is 2 dB, and the beam coupling loss attributed to spillover and mutual coupling is negligible.

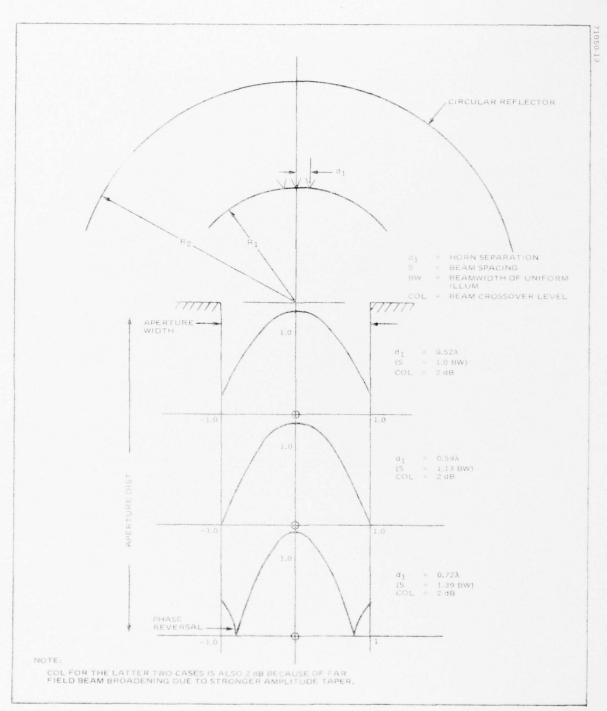
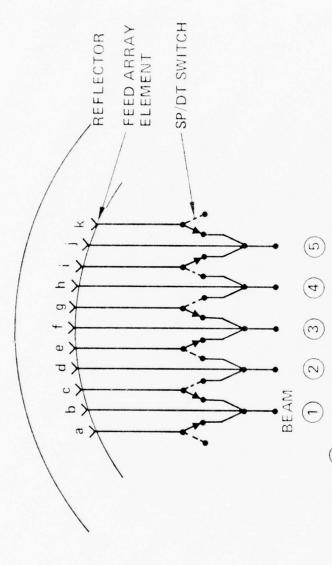


Figure IV.18. Illustration on the Crossover Level Limitation Due to Block Feeding

It is apparent that high crossover level can be obtained without incurring large beam coupling loss in this block feeding approach.

An attempt was made to reduce the crossover level by increasing the feed array element spacing. It should be noted that crossover levels of 2 to 4 dB can be obtained for the single feed horn case by means of varying element spacing (see Figure IV.12.a. This attempt was unsuccessful for the block feeding case because the crossover level remains at 2 dB when element spacing is increased to 0.72λ . The limitation on crossover level due to this method of block feeding can be explained by referring to Figure IV.18, in which the aperture distributions are shown for element spacings of 0.52λ , 0.59λ and 0.72λ . The angular separation between adjacent beams has increased when the feed element spacing is increased from 0.52λ to 0.72λ ; however, there is a corresponding increase in beamwidth due to the increase in amplitude tapering for the larger element spacing. Apparently, the broadening in beamwidth cancels out the increase in beam separation so that the crossover level remains virtually unaffected.

It is possible to obtain crossover levels of less than 2 dB by employing three elements for each block-fed group as shown in Figure IV.19. The amplitude weighting applied to the three-element block can be varied to control the aperture distribution. The radiation patterns of a design with amplitude weighting coefficient of (0.25, 1.00, 0.25) have been computed and shown in Figure IV.20. The crossover level is 2.7 dB, and the sidelobe level is -28 dB. Other amplitude weightings were also investigated, and the results on crossover and sidelobe level are shown in Table 4.2. It can be observed that crossover levels of 1.7 to 3.4 dB can be obtained readily. The higher crossover levels are accompanied by higher sidelobes so that resistive tapering may be



BEAM (1) FEEDS FEED ARRAY ELEMENTS a, b, AND c,

BEAM 2) FEEDS FEED ARRAY ELEMENTS c, d, AND e, AND ETC.

NOTE THAT SELECTION OF BEAM 3 PREVENTS FORMATION OF BEAMS 2 AND 4

65315-34 (11-10-76)

FIGURE IV. 19 - BLOCK FEEDING OF THREE ELEMENTS TO FORM ONE BEAM,

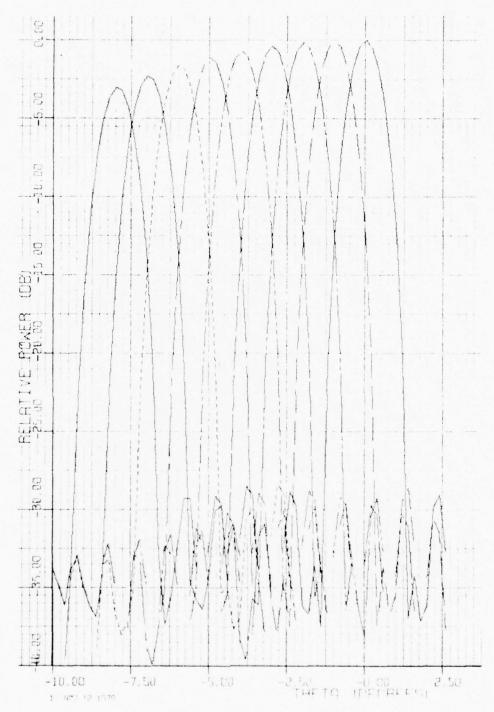


FIGURE IV.20 – FAR FIELD PATTERNS FOR BLOCK FEEDING OF THREE HORNS.

employed for additional sidelobe suppression. The disadvantage in the threeelement block feeding design is the added complexity in the power divider, and the doubling of the number of required feeding elements in each pillbox. An alternative scheme of providing block feeding in the beam switching matrix is also available. This will be discussed further in later sections when the beam switching matrix design is discussed.

TABLE 4.1 – SUMMARY OF CROSSOVER AND SIDELOBE LEVEL FOR THREE-HORN BLOCK FEEDING.

| Case | Beam Spacing | Amplitude Weighting | Beam Crossover Level | Sidelobe Level |
|------|--------------|------------------------|-------------------------|----------------|
| 1 | 10 | .45,1.,.45 | 1.7 dB | 33 dB |
| 2 | 10 | .25,1.,.25 | 2.7 dB | 28 dB |
| 3 | 10 | .20,1.,.20 | 3.0 dB | 26 dB |
| 4 | 10 | .15,1.,.15 | 3.4 dB | 22 dB |
| | | | | |

(no resistive taper applied)

Pillbox Design for the Above Data

- 1. Radiating aperture = $30 \times 2.064 \lambda = 61.92 \lambda$
- 2. Pillbox radius: $R_2 = 18.5\lambda$, $R_1 = 9.75\lambda$
- 3. Pickup aperture = 16.5λ
- 4. Maximum scan angle in the pillbox = 36° (for 9° beam) Scan angle = 31.5° for 8° beam in space
- 5. The horns are spaced so that their beams are I apart in space

V. ALTERNATE MULTIPLE BEAMFORMING MATRIX (CONSTRAINED LENS)

A. Description of the Multiple Beam Constrained Lens

It is well known that reflector antennas can be scanned by a physical displacement of the feed. In the case of a spherical reflector, spherical aberration phase error exists for all scan angles. However, the scannable range is quite large. When many feed horns are located in front of the reflector to form multiple beams, they cause aperture blockage. In general, this problem is a severe limiting factor when the number of feed horns is large as in a typical multiple beam antenna design.

A simple solution to the aperture blockage problem is the offsetting of the feed with respect to the reflector. Other solutions to this blockage problem have been developed by Hughes Aircraft Company in the HIHAT antenna and the multiple beam constrained lens. In the HIHAT antenna, as shown in Figure V.1, the array of feed horns is made transparent by the application of dual circular polarization in a duplexing array. In this duplexing array one sense of circular polarization is used for transmission to the reflector and the orthogonal sense is used to receive the reflected wavefront from the reflector. The receive signals are transmitted to a transfer array for re-radiating into space. In the multiple beam constrained lens which is really a derivative of the HIHAT Lens (as shown in Figure V.2), the blockage problem is avoided by replacing the spherical reflector by means of two spherical array surfaces with equal interconnecting cables. In this manner, both devices can be used as multiple beam matrices.

The multiple beam constrained lens as utilized in the present application is shown in Figure V.3. Essentially, it replaces the two sets of stacked pillboxes.

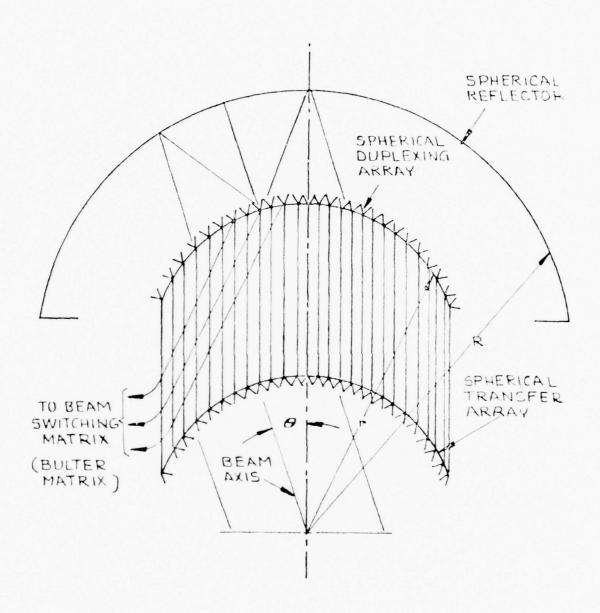
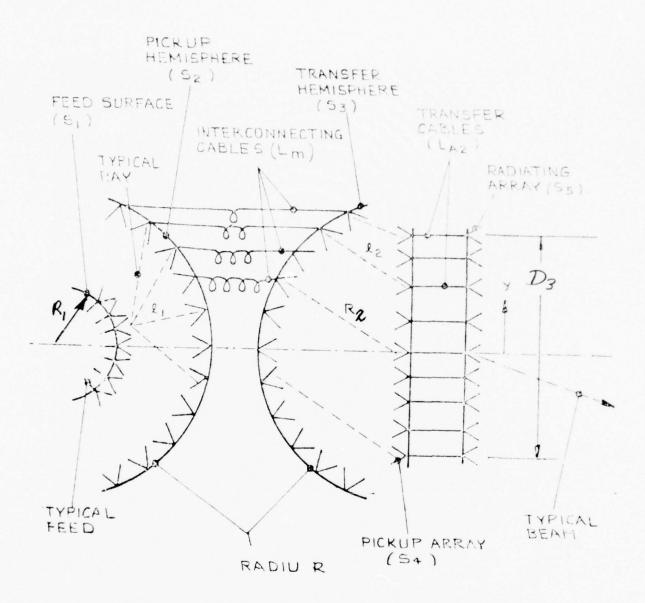
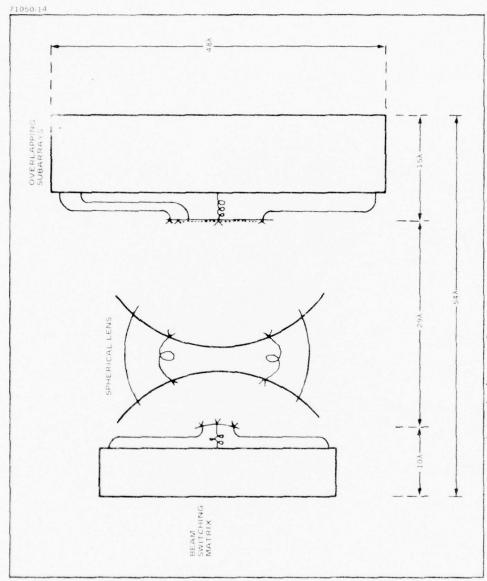


FIGURE V.1 - THE HIHAT ANTENNA AS A MULTIPLE BEAM DEVICE.



8=l1+l2-(1+R) AT 0=0 IF Lm's ARE EQUAL

FIGURE V.2 - THE MULTIPLE BEAM CONSTRAINED LENS.



It shares the wideband characteristics of the stacked pillbox design in that the beams do not scan with frequency. It has the apparent advantage of requiring fewer components; however, the requirement of interconnecting cables between the two spherical arrays represents a rather significant disadvantage.

B. Optimal Selection of Lens Parameters

The design consideration of lens optics is parallel to that of the stacked pillbox. In fact, the phase error distribution of the spherical lens is identical to that of the pillbox when the proper equivalence is made on the distance variable. Thus, the selection of ${\bf R_1}$, ${\bf R_2}$, and ${\bf D_3}$ (see Figure V.2) follows the design data in Figures IV.3, IV.4, IV.5, and IV.6. As shown previously, the crossover level can be adjusted by either variation of feed horn spacing or the aperture diameter over spherical radius ratio. This procedure has been followed and some sample cases have been studied. In Figures V.4, V.5, and V.6, the radiation patterns for crossover levels of 2.2 dB, 3.0 dB, and 4.0 dB, respectively, are shown. The sidelobe level for all cases is about -14 dB; therefore, additional sidelobe suppression by means of block feeding on resistive tapering is also required. The dependence of beam coupling loss on crossover level is shown in Figure V.7. Comparison is made between this design and other possible designs such as the Butler matrix and the design employing stacked pillboxes. The result as obtained by Stein³ is also included for comparison. It can be observed from Figure V.7 that all curves with the exception of the case of the spherical constrained lens are very close together, which indicates that the Butler matrix and stacked pillboxes under optimum circuit matching conditions are close to perfect multiple beamforming devices. The spherical lens actually is also close to the same condition. The increase in beam

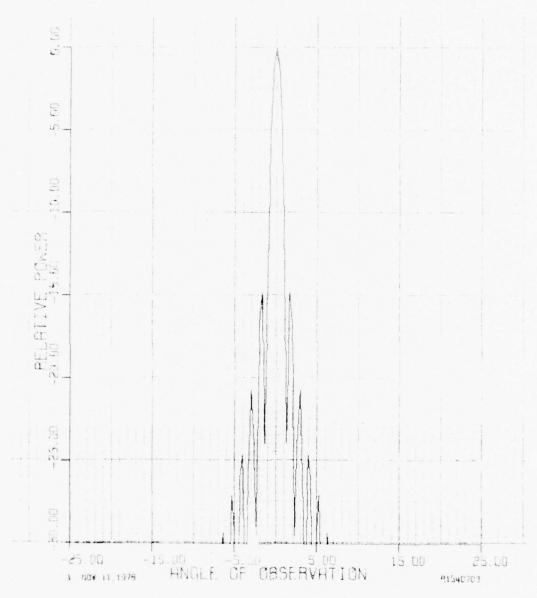


FIGURE V.4 – FAR FIELD PATTERN OF ARRAY WITH SPHERICAL LENS BEAMFORMER 2.2 dB BEAM CROSSOVER 3.1 dB BEAM COUPLING LOSS

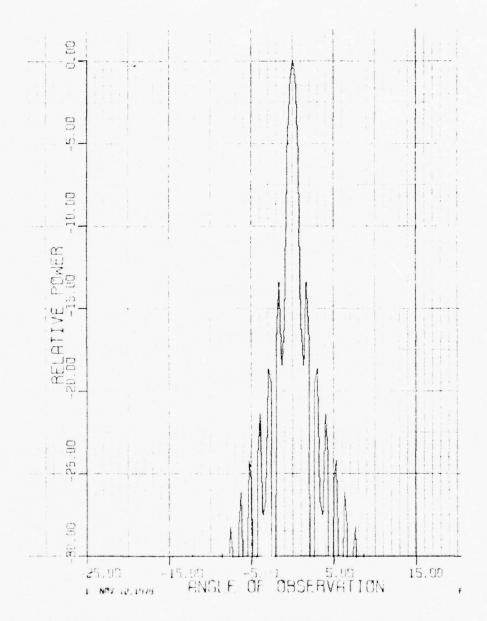


FIGURE V.5 – FAR FIELD PATTERN OF ARRAY WITH SPHERICAL LENS BEAMFORMER 3.0 dB BEAM CROSSOVER 1.55 BEAM COUPLING LOSS

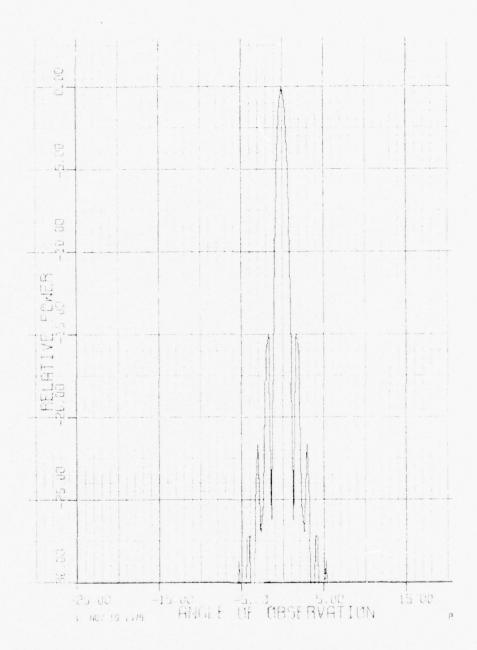
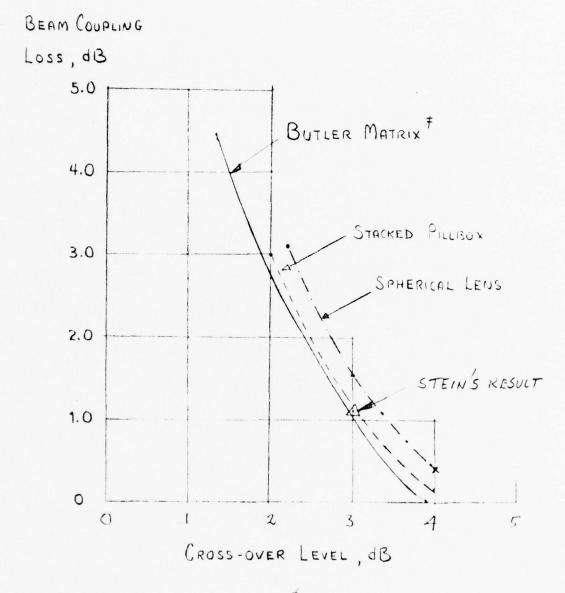


FIGURE V.6 - FAR FIELD PATTERN OF ARRAY WITH SPHERICAL - LENS BEAMFORMER
4.0 dB BEAM CROSSOVER
.4 dB BEAM COUPLING LOSS



To achieve non-orthogonal beam crossover end output ports are loaded.

FIGURE V.7 – COMPARISON OF BEAM COUPLING LOSS OF VARIOUS MULTIPLE BEAM DEVICES.

coupling loss of approximately 0.4 dB for the spherical lens arises at least in part from the fact that the aperture distribution generated by the spherical lens possesses slightly stronger taper in the diagonal cuts through the aperture. This effect manifests in the low sidelobes for this case. This fact can be observed by comparing Figure V.4 to IV.11.

C. Methods of Providing Sidelobe Control

Sidelobe suppression by means of block feeding and resistive tapering can be applied in the same manner as discussed in Section IV.E. It is expected that similar tradeoff in system complexity and antenna efficiency also applies in the present case.

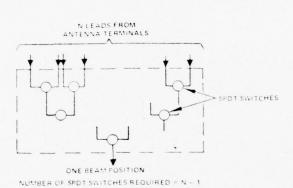
VI. BEAM SWITCHING MATRIX

A. Description of the Beam Switching Matrix Design Without Block Feeding

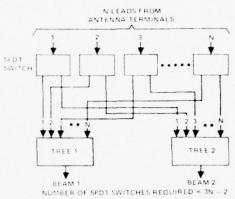
The first selection method to be considered connects a single receiver processing channel to one of N antenna terminals (output terminals of the multiple beam matrix). Figure VI.1.a shows a matrix of switches used to select a single receive beam from the N available beam position terminals at the antenna output. The matrix is a simple switching tree containing (N-1) single-pole, double-throw (SPDT) switching junctions. The number of switches required to select a single receive beam is thus nearly equal to the total number of receive beam positions.

Figure VI.1.b shows a matrix for selecting two receive beams simultaneously. Each antenna output terminal is connected to an SPDT switch which selects one of two switching trees for each of the antenna output leads. The outputs of these switches are connected to two switching trees, each of which is identical to that of Figure VI.1.a. The number of switches required for this two-beam matrix is (3N-2).

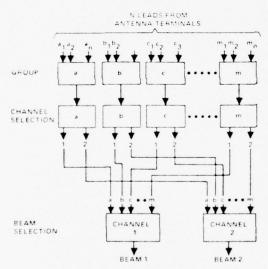
An important characteristic of the design in Figure VI.1.b is the independence of the two beam choices. With the SPDT switches at the N input beam positions, the choice of beam position for beam 1 does not affect the choice for beam 2. This method can be extended to S simultaneous beam selections, and the number of switches required as N(2S-1)-S. This method of beam switching is the most costly with respect to numbers of required switches. This high cost can be attributed to the independence of choice of the several selected beams.



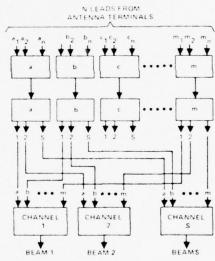
(a) SWITCHING MATRIX USED TO SELECT ONE BEAM POSITION FROM A TOTAL OF N AVAILABLE BEAM POSITIONS



(b) SWITCHING MATRIX USED TO SELECT TWO SIMULTANEOUS BEAM POSITIONS THE TWO SWITCHING TREES ARE IDENTICAL TO THAT SHOWN IN FIG. 1



NUMBER OF SPDT SWITCHES REQUIRED = $N(1 + \frac{2}{n}) - 2$



NUMBER OF SPDT SWITCHES REQUIRED - N [1 + $\frac{2}{n}$ (S - 1)] - S

 (ϵ) alternate switching matrix for the selection of two simultaneous beam positions. The two beams cannot be selected from the same group

(d) RECEIVER SWITCHING MATRIX USED TO SELECT S SIMULTANEOUS RECEIVE BEAM POSITIONS

65315-33 (11-10-76)

FIGURE VI.1 - DESIGN PRINCIPLE OF THE SWITCHING MATRIX.

An alternate method of selecting two simultaneous receive beams is shown in Figure VI.1.c. In this design, the N inputs are divided into m groups of n beam positions per group (mn = N). The first level of switching contains m switching trees with n-1 SPDT switches in each tree. This level selects one beam position for each group of n inputs resulting in m outputs from this switching level. The second level of switching selects one of the two receiver switching trees for each of the m leads, and the third level of switching selects one of the m beam positions for each of the two simultaneous receive beams. The second and third levels of switching are entirely analogous to the selection method of Figure VI.1.b, with the exception that the input has m leads instead of the N leads of Figure VI.1.b. The number of SPDT switches required for selecting two simultaneous receive beams using the grouping method of Figure VI.1.c is $N\{1 + (2/n)\}$ - 2. This requirement is nearly one-third the number of switches required for the matrix of Figure VI.1.b depending on the number of beams in each group, n. The reduction in required number of switches can be attributed to a reduced flexibility of the selection operation. The matrix of Figure VI.1.b has the capability of selecting the two receive beams in a completely independent manner while the matrix of Figure VI.1.c is restricted to selecting the two beams in different groups. It can be seen that the larger the group (an increase of n), the less flexibility because of the increase in number of beams excluded from simultaneous selection.

The two-beam selection matrix presented in Figure VI.1.c can be extended to select S simultaneous receive beams. The matrix design which accomplishes this is shown in Figure VI.1.d. As in the two-beam matrix, the first level of S beam matrix selects m beam positions from the total N inputs by selecting a single beam from each of the m groups of n inputs per group. Referring to Figure VI.1.d, the second level of the matrix selects one

of the S channels for each of the m first level outputs. The third level of switching then selects the S simultaneous beams which appear at the output of the matrix. With this matrix design, the second and third levels of switching allow any one of the m first level outputs to be routed to any one of the S output lines. The number of switching junctions required for this design which selects S simultaneous independent receive beams can be shown to be the following:

Number of SPDT switches =
$$N\left\{1 + \frac{2}{n}(S-1)\right\}$$
 - S (6-1) where,

N = total number of receive beams available at the antenna output terminals

n = number of receive beams per group

 $S = number\ of\ simultaneous\ selected\ receive\ beams\ at\ the\ matrix$ output.

B. Beam Switching Matrix Design for Block Feeding

The design concept for the beam switching matrix without block feeding can be extended to the case of block feeding by the steps below:

- Subdivide the feed element locations into similar blocks of elements as shown in Figures VI.2.a, VI.2.b, and VI.2.c.
 Three examples are shown: the four-element group, the nineelement group, and the five-element group.
- 2. An element in a specific position within the block can be assigned to a set formed by other elements in the same position within the block. Thus, all elements in the upper left-hand corner of the four-element block form Set A, and all elements in the upper right hand corner of the four-element block form Set B, and so on.

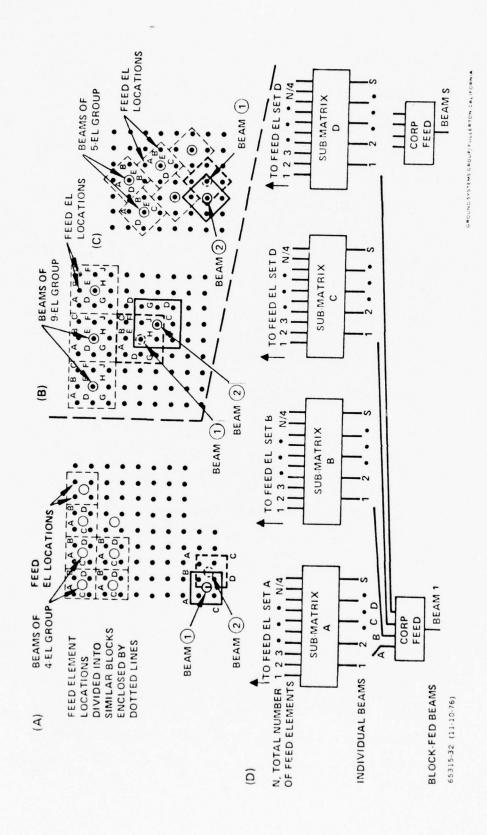


FIGURE VI. 2 - BEAM SWITCHING MATRIX DESIGN WITH BLOCK FEEDING.

- Feed elements in each set such as Set A are selected by a submatrix to form S simultaneous <u>individual</u> beams (see Figure VI.2.d).
- 4. An individual beam from each submatrix is combined with other individual beams from other submatrices in a corporate feed to form the required block-fed beam (see Figure VI.2.d). The design of the submatrices is identical to the design of the switching matrix in Figure VI.1.d. It is noted, however, that the total number of leads to each submatrix is reduced by a factor equal to the number of submatrices, or the number of feed elements in each block. In the case of the four-element group as shown in Figure VI.2.d, the total number of leads to each submatrix is $N_1/4$. For k element block, the number is N_1/k . It is also possible to reduce the required number of switches by trading off some flexibility in beam selection. We can form groups of n block-fed beams. Feed elements of Set A which are required to form each group of n block-fed beams are selected by the first level of submatrix A as shown in Figure VI.3. Feed element set B and others are selected in the same manner. It is important to note that the number of branches in each first level matrix is now n, which is equal to n/k. Other portions of the submatrix design are similar to the switching matrix of Figure VI.1.d.

The submatrices actually provide ks simultaneous beams. Any combinations of individual beams can be selected though only some of these are useful. In Figure VI. 2. a, Beam 1 is formed

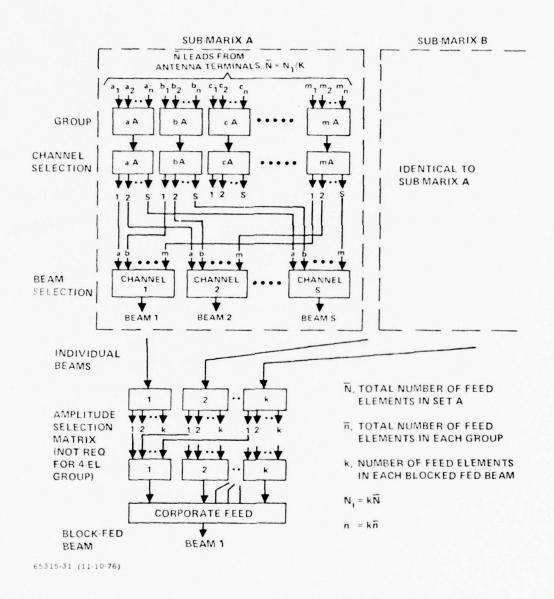


FIGURE VI. 3 - SUBMATRICES AND AMPLITUDE SELECTION MATRIX.

by selecting the individual Beams A, B, D, and C and Beam 2 is formed by selecting B, A, C, and D. The orientation of the individual beams with respect to each other is important in the event that unequal weighting is applied in the corporate feed. For the four element block, equal weighting is applied so that the orientation of the individual beams is not important. For the nine-element block, unequal weighting is used so that the orientation of the individual beams is very important. For example, refer to Figure VI. 2.b, Beam 1 is formed with individual beam E in the middle, and A, B, C, F, J. H. G, and D, counting from the upper left hand corner in a clockwise fashion. Beam 2 is formed with individual beam J in the middle, and E, F, D, G, A, C, B and H also counting from the upper left-hand corner clockwise. In order to provide the proper weighting to the individual beams, the sequence in Beam 2 must be rearranged to the same sequence as for Beam 1, the amplitude selection matrix as shown in Figure VI. 3 is used to accomplish this function. As a result, both the four-element block and the nine-element block can provide beam separation given by the individual beams. It is obvious from examination of Figure VI.2.c that the beam switching matrix for the five-element block can be designed in the same manner.

The number of switching junctions required for the submatrices can be determined as follows:

Number of SPDT switches (submatrices) =

$$N_1 \left\{ 1 + \frac{2}{n} (S-1) \right\} - ks$$
 (6-2)

in which

K is the number of elements in a block,

N, is the total number of individual beams,

S is number of simultaneous beams, and

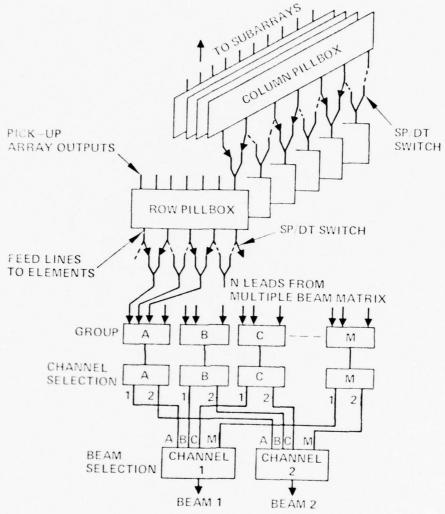
n is the number of individual receive beams per group in each submatrix

It is important to note that the total number of available block-fed beams is less than the total number of individual beams, and the number of block-fed receive beams in each group, n is equal to kn. The number of switching junctions required for the amplitude selection matrices is given below:

Number of SPDT switches (amplitude selection) = 2k(k-1) (6-3)

C. Alternate Beam Switching Matrix Design for Block Feeding

There exist many ways of designing the beam switching matrix to allow block feeding. In Figures VI.2 and VI.3, a method is shown in which individual beams are selected before combining in a corporate feed. In some cases, it is advantageous to form the block-fed beam before selection in the beam switching matrix. A straightforward approach of achieving this is shown in Figure VI.4, in which the block feeding scheme of Figure IV.17.c is incorporated into the beam switching matrix of Figure VI.1.c. It is obvious that in addition to the exclusion of simultaneous beams within the same group, this device also excludes the adjacent beams of a particular selected beam. However, if the beam positions within each group are contiguous, the added exclusion of adjacent beams does not reduce the beam selection flexibility significantly.



65315-30 (11-10-76)

FIGURE VI. 4 – ALTERNATE BEAM SWITCHING MATRIX DESIGN WITH BLOCK FEEDING OF 2 \times 2 ELEMENTS.

Even though Figure VI.4 shows block feeding of 2 x 2 elements, close examination of Figure VI.4 reveals that the same technique is also applicable to block size other than 2 x 2. The number of SPDT switches required for this design which selects S simultaneous independent receive beams are increased by 2N, in which N is the total number of receive beams (block-fed beams) at the antenna output terminals.

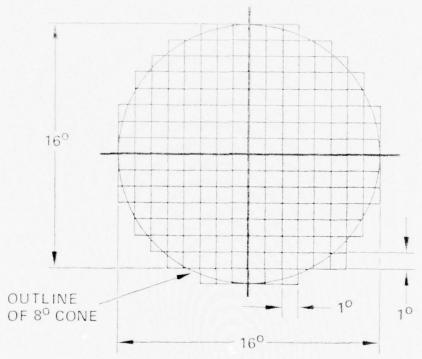
Number of SPDT Switches =
$$N\{3 + 2/n (S-1)\}$$
 - S (6-4)

In certain cases, this alternate design results in reduction of the number of switching junctions, but it also requires the receive signal to traverse more levels of switching junction so that the insertion loss is higher.

D. Typical Examples of Beam Switching Matrix

The design techniques for the beam switching matrix as discussed in the last sections are used for the 1° x 1° beam antenna with 3 dB crossover between adjacent beams. The beam position diagram for the 1° x 1° beam antenna with 8° half angle conical coverage is shown in Figure VI.5. The complexity of the beam switching matrix is proportional to the number of single pole double throw (SPDT) junctions. Certain beam exclusion was assumed to reduce the number of SPDT junctions. In a specific example as shown in Figure VI.6, the beam position diagram is divided into 13 groups with 16 beams in each group. The number of single pole double throw (SPDT) junctions required as given by equation (6-1) is 382. This switch matrix will allow 8 simultaneous beams to be selected from 8 of the 13 groups. However, for each beam, 15 positions within the same group are excluded for other simultaneous beams. Other grouping of the beam positions is also possible.

In general, the required number of SPDT junctions is reduced when the number of excluded beams increases as shown by the family of curves in



- 52 BEAM POSITIONS PER QUADRANT
- 208 BEAM POSITIONS WITHIN AN 8° CONE

FIGURE VI.5 - BEAM POSITION DIAGRAM.

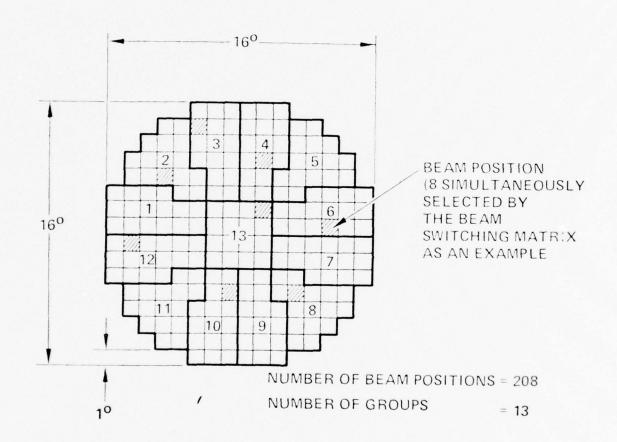


FIGURE VI. 6 - EXAMPLE OF DIVIDING COVERAGE INTO GROUPS.

Figure VI.7 with the number of simultaneous beams (S) as a parameter. It can be observed that the required number of SPDT junctions is greatly reduced when more beam position exclusions are permitted. For example, in the case of 8 simultaneous beams, without exclusion, 3112 SPDT junctions are required. This number reduces the 382 when 15 beam positions are excluded for each beam. Grouping for 32 simultaneous beams is shown in Figure VI.8. The grouping configuration is rather arbitrary and can be designed to reduce the effect of beam exclusions. For each combination of simultaneous beams and beam exclusions, the beam switching matrix design remains the same for all grouping configurations. The discussion in this section so far is also applicable for block feeding with the exception of the required number of SPDT switches. Consider the four-element block feeding design in which the beam switching matrix of Figure VI.2.d is used. For 8 simultaneous beams with 15 beam exclusion, the number of switches is now 1120 as compared to 382 in the absence of block feeding. When the alternate beam switching matrix of Figure VI.4 is used, the required number of switches is 798. Other cases are presented in Table VI.1. In all cases, block feeding increases the number of switching junctions required.

E. Estimated Losses in the Beam Switching Matrix

The insertion loss of the beam switching matrix is dependent on the following factors:

- 1. The total number of beam positions.
- 2. Number of simultaneous beams.
- 3. The number of beam exclusions.
- 4. Length of interconnecting cables.
- 5. Switch design.

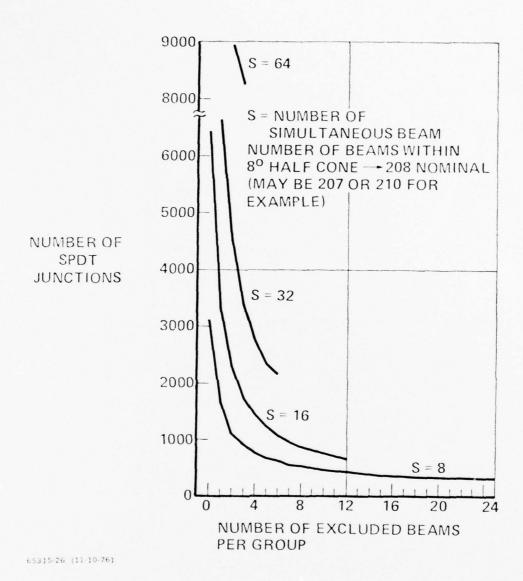


FIGURE VI.7 – NUMBER OF SPDT JUNCTIONS VS NUMBER OF EXCLUDED BEAM POSITIONS PER GROUP.

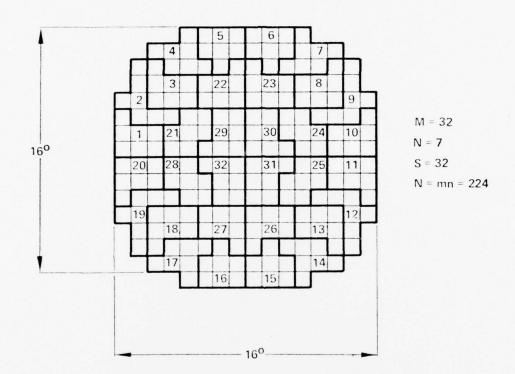


FIGURE VI.8 - GROUPING CONFIGURATION FOR CASE THREE.

TABLE VI. 1 – COMPARISON OF REQUIRED SWITCHING JUNCTIONS WITH AND WITHOUT BLOCK FEEDING.

Number of Beam Positions = 208 (256 for Block Feeding)

| No. of Simultaneous Beams | No. of Excl. Beams | 4-Element Block Feeding (Selection Before Beamforming) | 4-Element Block Feeding (Selection Aft r Beamforming) | Without Block Feeding |
|---------------------------------|--------------------------|--|---|--------------------------|
| 8 | 15 | 1120 | 798 | 382 |
| 32 | 3 | 16000 | 3816 | 3400 |
| 8 | 0 | 3808* | 3528* | 3112 |

^{*}Adjacent beams are excluded when block feeding is applied.

As a rule of thumb, the insertion loss of the switching matrix is proportional to the number of SPDT junctions which the signal is transmitted through. The number of SPDT junctions in cascade is dependent more on the required number of beam positions but less on the number of simultaneous beams or the number of exclusions as indicated below:

Total Number of Beam Positions = 208

| <u>s</u> | Number of Exclusion | Number of SPDT Junction in Cascade |
|----------|---------------------|---------------------------------------|
| 1 | 0 | 8 |
| 8 | 25 to 0 | 11 to 12 |
| 16 | 12 to 0 | 12 to 13 |
| 32 | 6 to 0 | 13 to 14 |
| 64 | 3 to 0 | 14 to 15 |

A large number of simultaneous beams in general increases the total line lengths of interconnecting cables required to connect the successive levels of switching trees. Referring to the schematic diagram in Figure VI.9, the cables connecting the second and the third levels must crisscross each other; thus they are relatively longer than other cables within the switching matrix.

Sample loss calculations on the switching matrix have been made. This switching matrix utilizes an X-band micromin switch built previously at Hughes Aircraft Company and .141" semi-rigid cables. It is also necessary to estimate the length of the cables from the schematic diagram in Figure VI.9. The estimated loss is in excess of 6 dB for all cases. Since insertion loss of this magnitude is not allowable in general, amplification may be required to circumvent loss in antenna gain due to this insertion loss component.

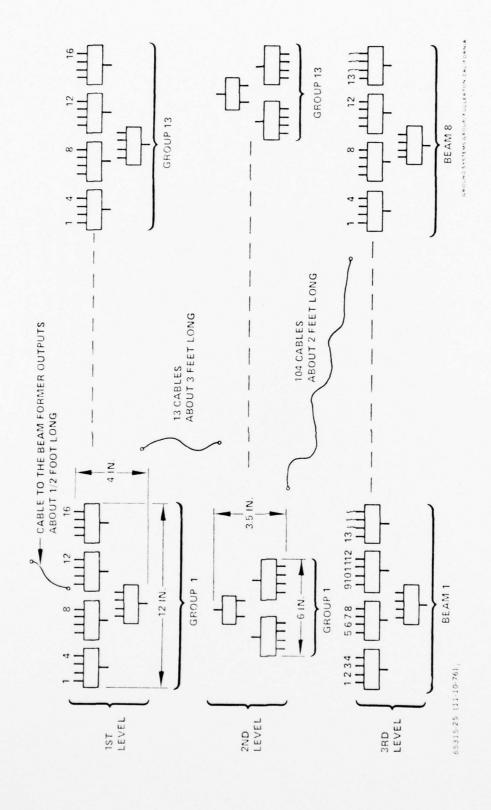


FIGURE VI, 9 - SCHEMATIC DIAGRAM FOR EIGHT SIMULTANEOUS BEAMS.

VII. SAMPLE MULTIPLE BEAM ANTENNA DESIGNS

Based on the analytical results obtained, two designs which meet the design specification in Section I have been worked out in detail. Design A employs single horn for each beam; thus, the sidelobe is only -13 dB. The radiation patterns for this design are shown in Figure IV.11. A scaled drawing of this design is shown in Figure VII.1 to indicate the overall size of the antenna system. Physical dimensions and parameters of the overlapping subarray, multiple beamforming matrix, and beam switching matrix are tabulated in Table VII.1. Two possible designs of the beam switching matrix are given: one with 8 independent beams, and the other with 16 independent beams. It is to be expected that the 8-beam design requires fewer components. Design B employs block feeding and resistive tapering to provide -30 dB sidelobe design. Two feed elements are driven in each of the stacked pillboxes so that the beam switching matrix of Figure VI.21.d is required. The radiation patterns in this case are shown in Figure IV.16. It can be seen that more components are required to provide an 8 independent beam design as compared to the Design A.

TABLE VII.1 - CHARACTERISTICS OF SAMPLE MULTIPLE BEAM ANTENNA (DESIGN A, 13 dB SL)

GENERAL

10 Beamwidth

8° half angle cone Scan Angle

Grating Lobe < 20 dB

Sidelobe -13 dB (see Figure IV.11)

Frequency 9500 MHz

1.240"

Overall Size $50\lambda \times 50\lambda \times 48\lambda$ or

62" x 62" x 59.5" (see Figure VII.1)

OVERLAPPING SUBARRAY

Element Spacing 0.52λ

Subarray Spacing 2.08λ

Number of Elements per Subarray

Number of Subarray Modules per Linear Array 25

Number of Overlapping Subarray PLA 24

Total Number of Overlapping Subarrays in the Entire Two Dimensional Arrays

576

Subarray Amplitude 0.1875, 0.400, 0.600, 0.8125, .8125, .600, .400, .1875

Total Number of Subarray Modules 3125

> First Level = 2500 Second Level = 625

Falloff in Subarray Factor at 8° Scan

3.0 dB

TABLE VII.1 (continued)

MULTIPLE BEAMFORMING MATRIX (STACKED PILLBOXES)

| Size of Unfolded Pillbox | 15λ x 25.5λ |
|---|---------------|
| Size of Folded Pillbox | 10λ x 25.5λ |
| Number of Input Terminals | 16 |
| Number of Output Terminals | 24 |
| Aperture Width of Pillbox | 13.3λ |
| Radius of Circular Reflector | 15 λ |
| Radius of Feed Array | 8λ |
| Element Spacing of Feed Array | 0.52λ |
| Chord Length of Reflector | 25.5λ |
| Number of Pillboxes First Level = 24 Second Level = 16 | 40 |
| Overall Depth of Multiple Beam Matrix (est.) | 23λ |
| Number of Beam Positions Available | 256 |
| Beam Position Lattice | Square |
| Number of Beam Positions with the 8º Half Angle Cone | 208 |
| Crossover Level Between Beams | 3 dB |
| Beam Coupling Loss | 1.2 dB |
| | |

TABLE VII.1 (continued)
BEAM SWITCHING MATRIX

| Design A1 (See Figure VI.25) | | Design A2 (See Figure VI.27) | |
|---|--------|---|------|
| No. of Independent Beams | 8 | No. of Independent Beams | 16 |
| No. of Beam Positions in a Group* | 16 | No. of Beam Positions in a Group | 7 |
| No. of SP/16T Switches | 13 | No. of SP/7T Switches | 32 |
| No. of SP/8T Switches | 13 | No. of SP/16T Switches | 32 |
| No. of SP/13T Switches | 8 | No. of SP/32T Switches | 16 |
| Total No. of SP/DT Switches for the Entire Switch Matrix | 382 | Total No. of SP/DT Switches for the Entire Switching Matrix | 1168 |
| Estimated Insertion Loss of BSM | 6.0 dB | | |

^{*}The number of unavailable beam positions after a beam is selected is given by the number of beam positions in a group minus one.

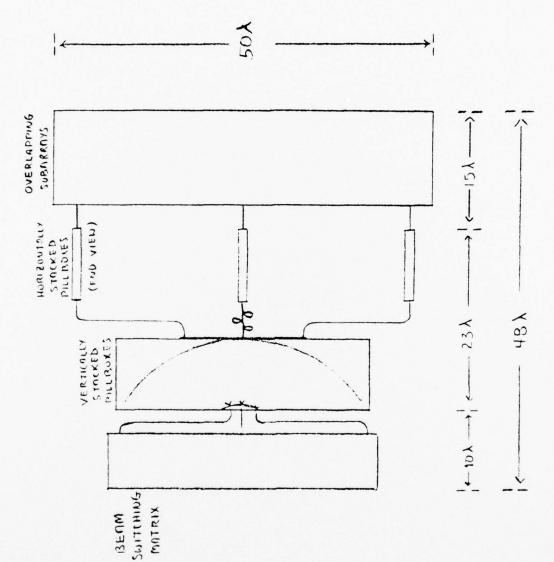


FIGURE VII.1 - SCALED DRAWING OF ANTENNA SYSTEM.

TABLE VII. 2 - CHARACTERISTICS OF SAMPLE MULTIPLE BEAM ANTENNA (Design B, -30 dB SL Obtained by Block Feeding and Resistive Tapering)

GENERAL

10 Beamwidth

80 half angle cone Scan Angle

Grating Lobe < 20 dB

Sidelobe -30 dB (see Figure IV.16)

Frequency 9500 MHz

1.240" λ_{o}

Overall Size $62\lambda \times 62\lambda \times 55\lambda$ or 76.9" x 76.9" x 68"

OVERLAPPING SUBARRAY

Element Spacing 0.52λ

Subarray Spacing 2.08λ

Number of Elements per Subarray 8

Number of Subarray Modules per Linear Array 31

Number of Overlapping Subarray PLA 30

Total Number of Overlapping Subarrays in the Entire Two

Dimensional Arrays 900

Subarray Amplitude 0.1875, 0.400, 0.600, 0.8125, .8125, .600, .400, .1875

Total Number of Subarray Modules 4805

First Level = 3844 Second Level = 961

Fall-off in Subarray Factor at

8º Scan 3.0 dB

TABLE VII.2 (continued)

Beam Coupling Loss

MULTIPLE BEAMFORMING MATRIX (STACKED PILLBOXES)

| Size of Unfolded Pillbox | 18.5λ x 31.4λ |
|---|----------------|
| Size of Folded Pillbox | 12. 3λ x 31.4λ |
| Number of Input Terminals | 20 |
| Number of Output Terminals | 30 |
| Aperture Width of Pillbox | 16.4λ |
| Radius of Circular Reflector | 18.5λ |
| Radius of Feed Array | 9 . 9λ |
| Element Spacing of Feed Array | 0.52λ |
| Chord Length of Reflector | 31.4\lambda |
| Number of Pillboxes First Level = 30 Second Level = 20 | 50 |
| Overall Depth of Multiple Beam Matrix (Est.) | 28λ |
| Number of Beam Positions Available | 400 |
| Beam Position Lattice | Square |
| Number of Beam Positions with the 8º Half Angle Cone | 324 |
| Crossover Level Between Beams | 2 dB |
| | |

1.4 dB (principally due to ohmic loss)

TABLE VII.2 (continued)

BEAM SWITCHING MATRIX

| Design B1 | | Design B2 | |
|---|--------|--|--------|
| Number of Independent Beams | 8 | Number of Independent Beams | 16 |
| Number of beam positions in a group* | 18 | Number of Beam Positions in a Group | 18 |
| Number of SP/18T Switches | 18 | Number of SP/7T Switches | 18 |
| Number of SP/8T Switches | 18 | Number of SP/16T Switches | 18 |
| Number of SP/18T Switches | 8 | Number of SP/18T Switches | 16 |
| Number of SP/DT Switches | 648 | Number of SP/DT Switches | 648 |
| Total Number of SP/DT Switches for the Entire Switch Matrix | 1216 | Total Number of SP/DT Switches for the Entire Switching Matrix | 1496 |
| Estimated Insertion Loss of BSM | 6.0 dB | Estimated Insertion Loss of BSM | 6.0 dB |

 $^{^{\}ast} \text{The number of unavailable beam positions after a beam is selected is given by number of beam positions in a group minus one.}$

VIII. CONCLUSIONS AND DISCUSSIONS

Based on the analytical study results obtained in this program, the following conclusions can be drawn:

- The described antenna technique can generate a large number of simultaneous independent beams over an 8° half angle cone.
- For a 1° beam antenna, the size of the multiple beam matrix is about 900 (30 x 30) instead of the usual 10,000 (100 x 100).
- The overlapping subarray technique suppresses the grating lobe to better than -20 dB, and its validity has been verified experimentally.
- Stacked pillboxes can be employed to form the multiple beam matrix with phase aberration less than 10°.
- Close-in sidelobes can be controlled to -30 dB by means of block feeding and resistive tapering.
- The design of the beam switching matrix to obtain 8 simultaneous independent beams is relatively simple. The switching network complexity grows when the required number of independent beams is large, or when the number of block feed horns is larger than four.

The recommended design to meet specific requirements of sidelobe and crossover level is tabulated in Table VIII.1. Block feeding is required for all low sidelobe designs.

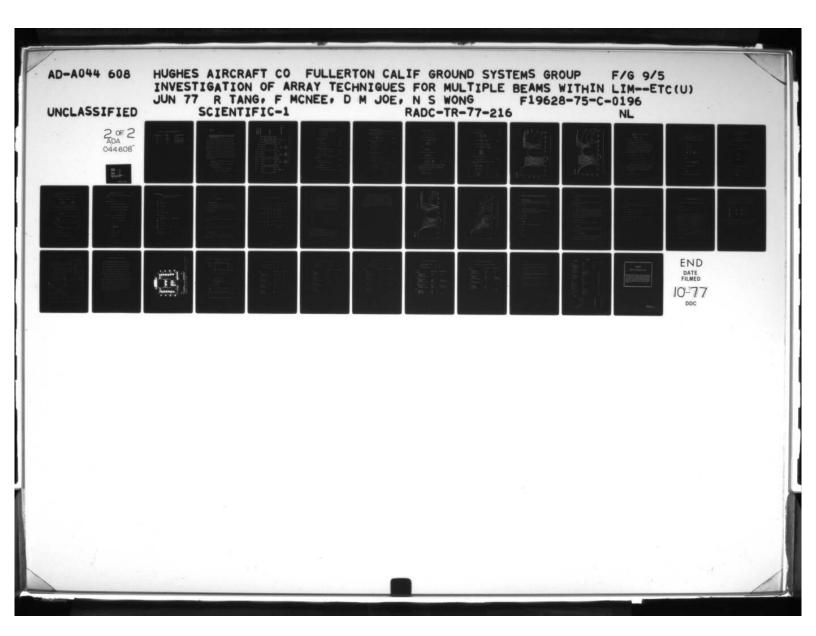


TABLE VIII.1 - SUMMARY OF RECOMMENDED DESIGNS.

| Crossover Level | Sidelobe | Recommended Design | |
|-----------------|----------|---|--|
| 3 d B | 13 dB | Single Beam | |
| 2 dB | 20-25 dB | Four Horn Block Feeding | |
| 2 dB | 30 dB | Four Horn Block Feeding and Resistive Tapering | |
| 3 dB | 30 dB | Nine Horn Block Feeding | |

IX. APPENDICES

APPENDIX A

1. Determination of Amplitude Weighting Coefficients and Definition of Feed Network to Meet Specific Requirements of Scan Coverage and Grating Lobe Suppression

Based on the network diagram in Figure A.1, it is required to define the coupling networks to meet specific requirements of scan coverage and grating lobe suppression. In addition, the subarray amplitude weighting coefficients, f_i , are to be determined. It is observed that the complete network comprises of 1:3 power dividers and 3:3 lossless multiple beam matrices. Idealized lossless couplers are presumed. Only symmetrical subarray amplitude distributions are of interest here for obvious reasons. To control the scan coverage, two nulls will be placed on the boundaries of the grating lobe region over the scan range. The problem will be solved in two steps: the constraints on the subarray amplitudes will be determined in the first step, and the effect on the subarray pattern will be studied in the next step to yield complete definition of the feed network to meet specific requirements on scan coverage and grating lobes.

a. Constraints on the Subarray Amplitudes by the Feed Network in Figure A $\,$

Refer to circuit diagram in Figure A.1, we can write out the following network equations:

For input from R terminal:

$$f_{2} = \{\cos \alpha_{1} \cos \alpha_{3} + j \sin \alpha_{1} \cos \alpha_{2} (j \sin \alpha_{3})\} R$$

$$f_{2} = (\cos \alpha_{1} \cos \alpha_{3} - \sin \alpha_{1} \cos \alpha_{2} \sin \alpha_{3}) R \qquad (A-1)$$

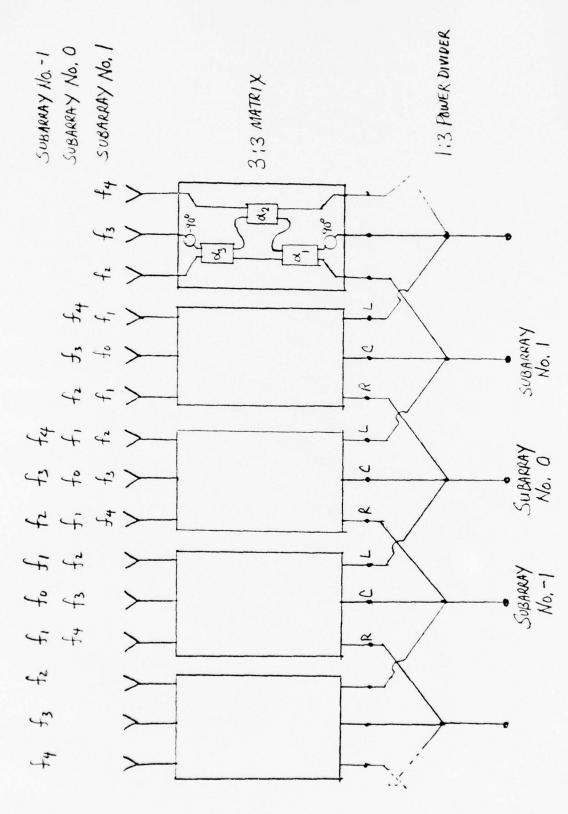


FIGURE A. 1 - DIAGRAM OF A THREE-LEVEL OVERLAPPING SUBARRAY.

$$\begin{split} &f_3 = \{\cos\alpha_1 \sin\alpha_3(-j) + j\sin\alpha_1 \cos\alpha_2(-j)\cos\alpha_3\} \, R \\ &f_3 = (\cos\alpha_1 \sin\alpha_3 + \sin\alpha_1 \cos\alpha_2 \cos\alpha_3) \, R \\ &f_4 = (j\sin\alpha_1 j\sin\alpha_2) \, R \\ &f_4 = (j\sin\alpha_1 j\sin\alpha_2) \, R \end{split} \tag{A-2}$$

For input from L terminal:

 $f_4 = (-\sin \alpha_1 \sin \alpha_2) R$

$$f_2 = (\cos a_2) L \tag{A-4}$$

(A-3)

$$f_3 = (\sin \alpha_2 \cos \alpha_3) L \tag{A-5}$$

$$f_4 = (-\sin \alpha_2 \sin \alpha_3) L \tag{A-6}$$

For input from C terminal:

$$f_1 = (-\cos \alpha_1 \cos \alpha_2 \sin \alpha_3 - \sin \alpha_1 \cos \alpha_3) C$$
 (A-7)

$$f_0 = (\cos \alpha_1 \cos \alpha_2 \cos \alpha_3 - \sin \alpha_1 \sin \alpha_3) C \tag{A-8}$$

$$f_1 = (-\cos \alpha_1 \sin \alpha_2) C \tag{A-9}$$

Only symmetrical distribution is allowable for symmetrical subarray patterns.

$$R=L (A-10)$$

From equations (A-3) and (A-6),

$$(-\sin \alpha_1 \sin \alpha_2) R = (-\sin \alpha_2 \sin \alpha_3) L$$

$$\alpha_1 = \alpha_3 \tag{A-11}$$

Substitute equation (A-11) into (A-1),

$$f_2/R = (\cos^2 \alpha_1 - \sin^2 \alpha_1 \cos \alpha_2) = 1 - \sin^2 \alpha_1 (1 + \cos \alpha_2)$$

Substitute equation (A-11) into (A-2)

$$f_3/R = (\cos \alpha_1 \sin \alpha_1 + \sin \alpha_1 \cos \alpha_2) = \cos \alpha_1 \sin \alpha_1 (1 + \cos \alpha_2)$$

Eliminate $\boldsymbol{\alpha}_{\!\!\!\!2}$ between the above two equations,

$$f_2/R = 1 - tan \alpha_1 f_3/R$$

$$\tan \alpha_1 = \frac{1 - (f_2/R)}{f_3/R} = (R - f_3)/f_3$$
 (A-12)

Combine equations (A-5) and (A-6),

$$\tan \alpha_3 = -f_4/f_3 \tag{A-13}$$

Combine (A-11), (A-12), and (A-13)

$$\frac{R}{f_3} - \frac{f_2}{f_3} + \frac{f_4}{f_3} = 0$$

$$L = R = f_2 - f_4 \tag{A-14}$$

Substitute equation (A-14) into (A-4)

$$\cos \alpha_2 = f_2/(f_2 - f_4)$$
 (A-15)

Combine equations (A-7) and (A-9),

$$-\cos\alpha_1\sin\alpha_2+\cos\alpha_1\cos\alpha_2\sin\alpha_3+\sin\alpha_1\cos\alpha_3=0$$

From equation (A-11), $\alpha_1 - \alpha_3$

$$-\cos\alpha_1\sin\alpha_2+\cos\alpha_1\cos\alpha_2\sin\alpha_1+\sin\alpha_1\cos\alpha_1=0$$

$$\sin \alpha_1 = \frac{+\sin \alpha_2}{1 + \cos \alpha_2} \tag{A-16}$$

It should be noted that both $\sin\alpha_1$ and $\sin\alpha_2$ possess the same sign.

From equations (A-8) and (A-11),

$$f_0/C = \cos^2\alpha_1 \cos\alpha_2 - \sin^2\alpha_1$$

$$f_0/C = \cos^2 \alpha_1 (1 + \cos \alpha_2) - 1$$

Substitute in equations (A-2) and (A-11)

$$f_0/C = \cos^2\alpha_1 \left(\frac{f_3/R}{\cos\alpha_1 \sin\alpha_1}\right) - 1$$

$$f_0/C = \left(\frac{f_3/R}{\tan \alpha_1}\right) - 1$$

Solve for C,

$$C = \frac{f_0 \tan \alpha_1}{b_3/R - \tan \alpha_1}$$

Substitute in R from equation (A-14)

$$C = \frac{f_0 (f_2 - f_4)}{f_3 \cot \alpha_1 - (f_2 - f_4)}$$

Substitute in $\tan \alpha_1$ from equation (A-13)

$$C = \frac{-f_0 f_4 (f_2 - f_4)}{f_3^2 + f_4 (f_2 - f_4)} = \frac{f_0 (f_2 - f_4)}{(f_2 + f_4)}$$
(A-17)

 α_1 can be computed from equation (A-16) or from a combination of equations (A-11) and (A-13). This redundancy may imply restrictions on the possible values of f_0 , f_1 , ... and f_4 . To eliminate possible inconsistancy, we proceed as follows:

$$\tan \alpha_1 = -f_4/f_3$$

$$\sin \alpha_1 = +\sin \alpha_2/(1 + \cos \alpha_2)$$

$$\cos \alpha_2 = f_2/(f_2 - f_4)$$

Manipulate equation (A-13).

$$\tan^{2}\alpha_{1} = \frac{\sin^{2}\alpha_{1}}{1 - \sin^{2}\alpha_{1}} = \left(\frac{f_{4}}{f_{3}}\right)$$

$$\sin^{2}\alpha_{1} = \frac{\left(f_{4}/f_{3}\right)^{2}}{1 + \left(f_{4}/f_{2}\right)^{2}} = \frac{f_{4}^{2}}{\frac{f_{2}^{2} + f_{4}^{2}}{f_{2}^{2} + f_{4}^{2}}} \tag{A-18a}$$

We also manipulate equations (A-15) and (A-16),

$$\sin^{2}\alpha_{1} = \frac{\sin^{2}\alpha_{2}}{(1 + \cos\alpha_{2})^{2}} = \frac{1 - \cos^{2}\alpha_{2}}{(1 + \cos\alpha_{2})^{2}}$$
$$= \frac{1 - \left(\frac{f_{2}}{f_{2}^{-1}f_{4}}\right)}{1 + \left(\frac{f_{2}}{f_{2}^{-1}f_{4}}\right)}$$

 $\sin^2\!\alpha_{\!1}$ can be simplified as follows:

$$\sin^2 \alpha_1 = -f_4/(2f_2 - f_4)$$
 (A-18b)

 $\sin^2\!\alpha_1^{}$ can be eliminated from the expressions in equations (A-18a) and (A-18b).

$$\frac{f_4^2}{f_3^2 + f_4^2} = \frac{-f_4}{(2f_2 - f_4)}$$

$$f_4(2f_2 - f_4) + f_3^2 + f_4^2 = 0$$

$$2f_2f_4 + f_3^2 = 0$$

$$f_3 = \pm \sqrt{-2f_2f_4}$$
(A-19)

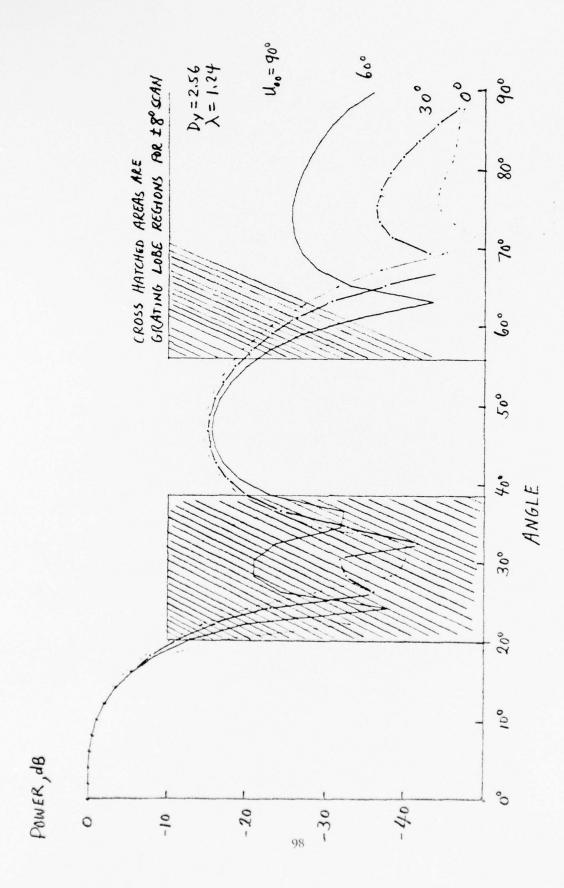


FIGURE A.2 - SUBARRAY PATTERNS OF GENERALIZED OVERLAPPING ARRAY.

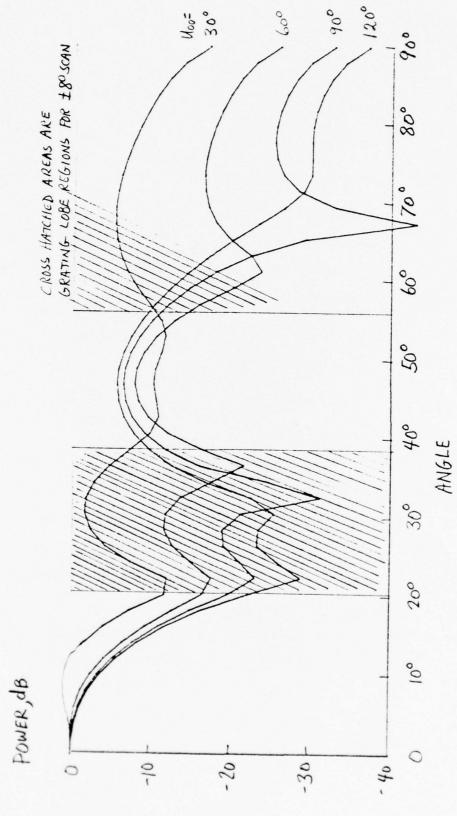


FIGURE A. 3 - SUBARRAY PATTERNS OF GENERALIZED OVERLAPPING SUBARRAY (SECOND SOLUTION).

$$f_{1} = \sqrt{\frac{2f_{2}}{(2f_{2} - f_{4})}} (2f_{2} - f_{4})(-f_{4}) \frac{1}{f_{2} - f_{4}} \frac{f_{0}(f_{2} - f_{4})}{(f_{2} + f_{4})}$$

$$f_{1} = \frac{\sqrt{-2f_{2}f_{4}}}{f_{2} + f_{4}} \frac{f_{0}}{f_{0}} = \frac{-f_{3}f_{0}}{f_{2} + f_{4}}$$
(A-20)

To have positive f, either f_3 or (f_2+f_4) are negative.

b. Constraints in f to Provide Required Subarray Patterns

So far f_1 and f_3 can be shown to be dependent on f_0 , f_2 , and f_4 . The three independent parameters f_0 , f_2 , and f_4 may be selected to provide the required subarray pattern shape. It is possible to select them so that at the scan limits, all grating lobes are coincident with subarray pattern nulls. When this condition is met, the amplitude and phase distribution of the array is that of a uniform plane wave:

$$a_0 = f_3 e^{jU_{00}} + f_0 + f_3 e^{-jU_{00}} = 1$$
 (A-21)

$$a_1 = f_2 e^{jU_{00}} + f_1 + f_4 e^{-jU_{00}} = e^{jU_{00}/3}$$
 (A-22)

$$a_{-1} = f_2 e^{-jU_{00}} + f_1 + f_4 e^{+jU_{00}} = e^{-jU_{00}/3}$$
 (A-23)

In the above formula, U_{oo} is the incremental phase between subarrays and $U_{oo}/3$ is the incremental phase between elements at a scan angle where all nulls are coincident with grating lobes. This condition also implies that the gain of the subarray factor is maximum.

Let
$$z = e^{\int U_{00}}$$

then $z^{-1} = e^{\int U_{00}}$, $z + z^{-1} = 2 \cos U_{00}$.

- sign should be chosen as seen later.

The f's cannot be independently chosen; they must be selected in accordance with equation (A-19). Either equation (A-16) or (A-19) can be regarded as the equation of constraint imposed by the network.

Additional constraint on the selection of f's can be derived from equations (A-7) or (A-9). f_1 can be determined from equation (A-9) as follows:

$$f_1 = -(\cos \alpha_1 \sin \alpha_2) C$$

$$\cos\alpha_1 = \sqrt{1 - \sin^2\alpha_1}$$

Substitute in equation (A-18b),

$$\cos \alpha_1 = \sqrt{1 - \frac{-f_4}{2f_2 - f_4}} = \sqrt{\frac{2f_2}{2f_2 - f_4}}$$

From equation (A-15),

$$\cos \alpha_2 = \frac{f_2}{f_2 - f_4}$$

$$\sin \alpha_2 = \sqrt{1 - \cos^2 \alpha_2} = \sqrt{1 - \left(\frac{f_2}{f_2 - f_4}\right)^2}$$

$$\sin\alpha_2 = \frac{1}{{\rm f_2}^-{\rm f_4}} \sqrt{(2{\rm f_2}^-{\rm f_4})(-{\rm f_4})}$$

From equation (A-17)

$$C = \frac{f_0(f_2 - f_4)}{(f_2 + f_4)}$$

Substitute $\cos \alpha_1$, $\sin \alpha_2$, and C into expression for f_1 ,

Equation (A-23) can be seen to be redundant.

$$f_0 + f_3 z + f_3 \frac{1}{z} = 1$$
,

$$f_1 + f_2 z + f_4 \frac{1}{z} = z^{1/3}$$

Resolve the above two equations into real and imaginary parts:

$$f_0 + 2 \cos U_{00} f_3 = 1$$

$$f_1 + f_2 \cos U_{00} + f_4 \cos U_{00} = \cos \frac{U_{00}}{3}$$

$$f_2 \sin U_{oo} - f_4 \sin U_{oo} + \sin \frac{U_{oo}}{3}$$

Define

$$S_1 = \frac{\sin \frac{U_{oo}}{3}}{\sin U_{oo}}$$

$$S_2 = \frac{\cos \frac{U_{oo}}{3}}{\cos U_{oo}}$$

and

$$\sigma = \sec^2 U_{oo}$$

We can rewrite the above equations as follows:

$$f_2 - f_4 = S_1$$
 (A-24)

$$\sqrt{\circ} f_1 + f_2 + f_4 = S_2 \tag{A-25}$$

$$f_0 + \frac{2}{\sqrt{\sigma}} f_3 = 1$$
 (A-26)

These equations would assume the coincidence of grating lobes with subarray pattern nulls at $U = U_{00}$.

Previously, we had derived the equation of orthogonality.

$$f_3 = -\sqrt{-2f_2f_4}$$
 or $+\sqrt{-2f_2f_4}$

$$f_1 = + \frac{f_0 \sqrt{-2f_2f_4}}{(f_2 + f_4)}$$
 or $- \frac{f_0 \sqrt{-2f_2f_4}}{(f_2 + f_4)}$

Intuitively, f_3 should be negative for better pattern control. Now, we have five equations and five unknowns in f_0 , f_1 , f_2 , f_3 , and f_4 .

First, f_3 can be eliminated by combining equations (A-26) and (A-19).

$$f_0 - \frac{2}{\sqrt{3}} = \sqrt{-f_2 f_4} = 1$$
 (A-27)

Secondly, f_0 can be eliminated from equations (A-20) and (A-27).

$$\frac{\sqrt{-2f_2f_4}}{(f_2+f_4)} = 1 + \frac{2}{\sqrt{2}} -2f_2f_4 \tag{A-28}$$

Furthermore, \mathbf{f}_1 can be eliminated by substituting \mathbf{f}_1 in equation (A-28) into equation (A-25).

$$\frac{\sqrt{-2f_2f_4}}{(f_2 + f_4)} \left(\sqrt{\sigma} + 2 \sqrt{-2f_2f_4} \right) + f_2 + f_4 = S_2$$
 (A-29)

Manipulating on equation (A-29),

$$\sqrt{-2f_2f_4} - 4f_2f_4 + (f_2 + f_4)^2 = S_2(f_2 + f_4)$$

$$\sqrt{5}$$
 $-2f_2f_4 = S_2(f_2 + f_4) - (f_2f_4)^2$

$$\sqrt{-2f_2f_4} = S_2(f_2 + f_4) - S_1^2$$
 (A-29a)

Finally we proceed to eliminate f_4 by combining equation (A-29a) and (A-24).

$$f_4 = f_2 - S_1$$

Squaring equation (A-29a):

$$\begin{aligned} -2 \circ f_2 f_4 &= S_2^2 (f_2 + f_4)^2 + S_1^4 - 2 S_2 S_1^2 (f_2 + f_4) \\ -2 \circ f_2 (f_2 - S_1) &= S_2^2 (2 f_2 - S_1)^2 + S_1^4 - 2 S_2 S_1^2 (2 f_2 - S_1) \\ -2 \circ f_2^2 + 2 \circ S_1 f_2 &= S_2^2 + f_2^2 + S_2^2 S_1^2 - 4 f_2 S_1 S_2^2 + S_1^4 \\ &- 4 S_2 S_1^2 f_2 + 2 S_2 S_1^3 \end{aligned}$$

Collecting terms, we get a quadratic equation in f₂.

$$(2^{\circ} + 4S_2^2) f_2^2 + (-2^{\circ}S_1 - 4S_1S_2^2 - 4S_1^2S_2) f_2$$

 $+ (S_1^2 + S_1S_2)^2 = 0$

$$Af_2^2 + Bf_2 + D = 0$$

$$f_2 = \frac{(-B \pm \sqrt{B^2 - 4AD)}}{2A}$$
 (A-30)

$$A = 2^{\circ} + 4S_2^2 \tag{A-31}$$

$$B = -2 S_1 - 4S_1 S_2^2 - 4S_1^2 S_2$$

$$D = (S_1^2 + S_1 S_2)^2$$

Summary of Results

Given: U_{oo}, Phase Shift between subarrays so that grating lobes coincide with subarray pattern nulls.

$$\begin{cases} \sigma = \sec^{2}(U_{oo}) \\ S_{1} = \sin \frac{U_{oo}}{3} / \sin(U_{oo}) \\ S_{2} = \cos \frac{U_{oo}}{3} / \cos(U_{oo}) \\ \end{cases}$$

$$\begin{cases} A = 2^{\circ} + 4S_{2}^{2} \\ B = -2^{\circ}S_{1} - 4S_{1}^{2}S_{2}^{2} - 4S_{1}^{2}S_{2} \\ D = (S_{1}^{2} + S_{1}S_{2})^{2} \end{cases}$$

$$\begin{cases} f_{2} = (-B + \sqrt{B^{2} - 4AD}) / (2A), & \text{or} \quad (-B - \sqrt{B^{2} - 4AD}) / (2A) \\ f_{4} = f_{2} - S_{1} \\ f_{0} = 1 - 2 \cos U_{oo} f_{3} \\ \end{cases}$$

$$\begin{cases} f_{3} = -2f_{2}f_{4}, & \text{or} \quad + -2f_{2}f_{4} \\ f_{1} = -f_{0}f_{3} / (f_{2} + f_{4}) \\ C = f_{0}(f_{2} - f_{4}) / (f_{2} + f_{4}) \\ C = R = f_{2} - f_{4} \end{cases}$$

$$\begin{aligned} &\tan\alpha_1 = \tan\alpha_3 = -f_4/f_3\\ &\cos\alpha_2 = f_2/(f_2-f_4)\\ &\sin\alpha_2 = \sin\alpha_1 \cdot \text{ABS} \left(\sqrt{1-\cos^2\alpha_2/\sin\alpha_1}\right) \end{aligned}$$

2. Grating Lobe Locations

The grating lobes must be suppressed by the subarray pattern in order to assure low sidelobe operation. To estimate the resultant sidelobe level, it is only necessary to determine the location of the grating lobes and the value of the subarray pattern at the grating lobe locations. The grating lobes are given by the following formula:

$$e^{jkDy(\sin\theta_S^{-}\sin\theta_m)} = 1$$

or

kDy
$$(\sin \theta_s - \sin \theta_m) = 2n\pi$$

The integer n gives the numbering index of the grating lobe. n=0 gives the main beam. Solving for $\theta_{\rm g}$,

$$\sin \theta_{s} = \frac{n\lambda}{Dv} + \sin \theta_{m}$$

The relation, $k=2\pi/\lambda$, has been used. The grating lobe locations for scan angles of -8° , 0° and $+8^{\circ}$ are tabulated in Table A.1 with element spacing as a parameter.

3. Numerical Results

A series of subarray amplitude distributions were computed from the derived results in the previous sections; furthermore, the far field subarray patterns were also computed. The first set of subarray patterns as shown in

TABLE A.1 – GRATING LOBE LOCATIONS

| | | | | | | =1391 = -8° | | |
|------------------|---|-----------------------|----------------------|--------|----------------------|----------------|----------------------|-----------------------|
| $\lambda = 1.24$ | n | $\frac{n\lambda}{Dy}$ | $\sin\theta_{\rm S}$ | s | $\sin\theta_{\rm S}$ | θs | $\sin\theta_{\rm S}$ | $\theta_{\mathtt{S}}$ |
| Dy = 2.56 | 1 | .4843 | .4843 | 28.96° | .3452 | 20.19° | .6235 | 38.56° |
| | 2 | .9687 | .9687 | 75.62° | .8296 | 56.05° | 1.1078 | |
| Dy = 2.41 | 1 | .5145 | .5145 | 30.96 | •3754 | 22.05 | .6535 | 40.80 |
| | 2 | 1.029 | 1.029 | > 900 | .8899 | 62.86 | | |
| Dy = 2.26 | 1 | .5486 | .5486 | 33.27 | .4095 | 24.17 | .6877 | 43.44 |
| | 2 | 1.097 | | | •9579 | 73.31 | | |
| Dy = 2.11 | 1 | .5876 | .5876 | 35.98 | .4485 | 26.64 | .7267 | 46.61 |
| -, | 2 | 1.175 | | | | | | |
| Dy = 2.71 | 1 | .4575 | .4575 | 27.23 | .3184 | 18.56q | .5966 | 36.62 |
| -1 - cilt | 2 | .915 | | | .7759 | 50.88 | | |

Figures A.2 and A.3 are for perfect coincidence of grating lobes and subarray pattern nulls at various scan angles in which the progressive phase is U. The subarray patterns in Figure A.2 are for negative values of f_3 , and those in Figure A.3 are for positive values of f_3 . The cross hatched areas are angular sectors which contain the grating lobes. From observation of the subarray pattern shape, it is apparent that negative values of f_3 are preferred over positive ones. In addition, U_{oo} cannot exceed 60° if the first sidelobe of the subarray pattern is to be under -20 dB. In any case, none of the possible cases can provide grating lobes of -20 dB.

Slight perturbation of amplitude weighting coefficients are possible by altering the coupling coefficients of the 1:3 power divider in the following manner:

$$f_0 = vf_0$$

$$\mathbf{f}_2 \stackrel{\rightarrow}{-} \mathbf{f}_2$$

$$f_3 \rightarrow f_3$$

$$f_4 - f_4$$

$$R - R$$

$$L \neg L$$

The 3:3 matrix remains unchanged.

The subarray patterns corresponding to $U_{oo} = 60^{\circ}$ for various perturbation factors, $^{\circ}$, are shown in Figure A.4. This slight perturbation on f's provides some equalization of the various grating lobe magnitudes. However, the additional benefit on grating lobe suppression is not significant.

It appears that the only effective means of obtaining grating lobe suppression of -20 dB is to reduce the element spacing. Figure A.5 gives the subarray patterns as a function of element spacing from 2.11 to 2.71 inches (λ = 1.24 inch). In all cases, the highest grating lobe falls within the main lobe of the subarray pattern. To obtain grating lobe suppression of -17 dB, element spacing of 2.11 inches must be used. Consequently, low grating lobe level is bought at significant reduction of element spacing or increase in the number of subarrays.

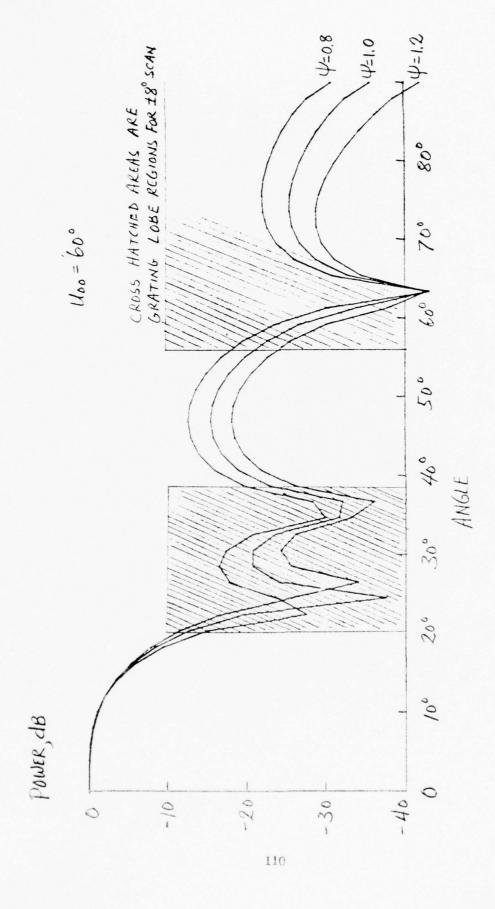


FIGURE A.4 - SUBARRAY PATTERNS OF GENERALIZED OVERLAPPING SUBARRAY ('OPTIMUM' C/R RATIO MULTIPLIED BY ")

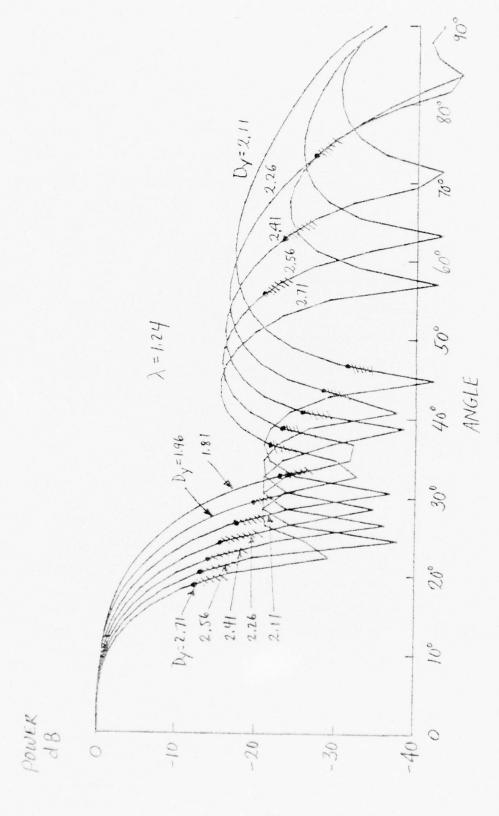


FIGURE A.5 — SUBARRAY PATTERNS OF GENERALIZED OVERLAPPING SUBARRAY (EFFECT OF SPACING ON GRATING LOBE SUPPRESSION)

APPENDIX B – DETERMINATION OF TRANSMISSION COEFFICIENT BETWEEN ELEMENTS IN FEED ARRAY AND RECEIVE ARRAY

1. Two-Dimensional Array

The power absorbed by a perfectly matched element in a two-dimensional array is equal to the incident power density times the elemental area. The antenna gain is therefore:

$$G = 4\pi A/\lambda^2 \tag{B-1}$$

where A is the effective area of the element.

The power transmission coefficient between an element in the feed array and an element in the pickup array is given by $Silver^6$ as:

$$\frac{P_r}{P_i} = \frac{G_t G_r \lambda^2}{16\pi^2 R^2}$$
(B-2)

Substitution of (B-1) gives:

$$\frac{P_r}{P_i} = \frac{A_r A_t}{R^2 \lambda^2}$$
 (B-3)

If a square element lattice is assumed, the pertinent areas are

$$A_t = \Delta^2$$

$$A_r = d^2$$

Consequently,

$$\frac{P_{r}}{P_{r}} = \frac{\Delta d^{2}}{R\lambda} \tag{B-4}$$

The transmission coefficient when the pertinent elements are directly facing each other is

$$g(m, p) = \frac{\Delta d}{R\lambda}$$
 (B-5)

In general, the line of sight is not normal to the plane of the arrays and (B-5) should be modified to yield

$$g(m, p) = \frac{\Delta d}{R\lambda} \cos \theta_1 \cos \theta_2 \tag{B-6}$$

In the above R is the distance between the two elements in question and θ , and θ_2 are the angles between line of sight and the normal to the arrays.

The factors $\cos\theta_1$ and $\cos\theta_2$ can be identified as the active element patterns of two arrays whose impedances are perfectly matched. In the event that the impedance of either one or both arrays are not matched, equation (B-6) can be generalized to include these cases:

$$g(m, p) = \frac{\Delta d}{R\lambda} S_1(\theta) \cdot S_2(\theta)$$
 (B-7)

In which $\mathbf{S}_1(\mathbf{\theta})$ and $\mathbf{S}_2(\mathbf{\theta})$ are the normalized active element patterns.

2. Linear Array

The derivation of the transmission coefficient in this case is parallel to that for the two-dimensional array. Assuming the radiation pattern to be given by (see Slater⁷),

$$F = \cos \theta = \frac{\sin(\pi d/\lambda) \sin \theta}{(\pi d/\lambda) \sin \theta}$$
(B-8)

Slater has shown that the radiation pattern of a rectangular area of uniform current distribution assumes the above form. Since the aperture with uniform distribution has maximum gain, the aperture is also matched.

The gain is

$$G = F^2/\overline{F^2} = 2\pi d/\lambda$$

or

$$d = \lambda/2\pi G \tag{B-9}$$

where $\overline{F^2}$ is the averaged power pattern.

It follows that the transmission coefficient in the case of normal incidence is,

$$g(m, p) = \frac{d\Delta}{R\lambda}$$
 (B-10)

For oblique incidence the above formula is modified to yield

$$g(m,p) = \frac{d\Delta}{R\lambda} \cos \theta_1 \cos \theta_2 \qquad (B-11)$$

When the arrays are not matched, the following formula must be used.

$$g(\mathbf{m}, \mathbf{p}) = \frac{d\Delta}{R\lambda} S_1(\theta) \cdot S_2(\theta)$$
 (B-12)

APPENDIX C – ACTIVE ELEMENT PATTERN OF AN ELEMENT IN THE REGULARLY SPACED ARRAY

It is well known that for a perfectly matched array, the element $gain^8$ is

$$g(\theta) = \frac{4\pi A}{\lambda^2} \cos \theta \tag{C-1}$$

Thus, the active element power pattern is

$$S^{2}(\theta) = \cos \theta \tag{C-2}$$

When the array is scanned over the angular range in which no grating lobes are formed, it is possible in principle to match the antenna array perfectly, and this perfectly matched condition is closely approached in practice. However, when grating lobes are formed, the antenna array on receive cannot be matched perfectly even though it may be perfectly matched on transmit. This phenomenon is quite analogous to the matching condition for a reactive tee junction in which the sum arm may be matched while the branch arms are not. The sum arm is equivalent to the transmission line mode within the feed lines of the antenna array, while the branch arms are equivalent to the space modes of the main beam and grating lobe. It has been our experience that antenna arrays can be matched on transmit in spite of presence of grating lobes. Under this matched condition, the active element pattern at scan angle in which the main beam and grating lobe are both at the same polar angle is given as

$$S^{2}(\theta)\Big|_{\theta=\theta_{1}} = \frac{\cos\theta_{1}}{2} \tag{C-3}$$

A well matched array in general possesses a well behaved active element pattern. Thus, it is reasonable to approximate the actual active element pattern by a straight line between the scan range of θ_0 to θ_1 , and perhaps slightly outside this range if necessary. θ_0 denotes the scan angle in which the grating lobe appears at endfire. To summarize, the empirical active element pattern is

$$S^{2}(\theta) = \cos \theta \qquad \qquad \theta < |\theta| \leq \theta_{0}$$

$$S^{2}(\theta) = \frac{\cos \theta_{1}}{2} + \left(\cos \theta_{0} - \frac{\cos \theta_{1}}{2}\right) \cdot \frac{\theta_{1} - \theta}{\theta_{1} - \theta_{0}}, \quad \theta_{0} < \theta \leq \theta_{1}$$

$$S^{2}(\theta) \cong \frac{\cos \theta_{1}}{2} + \left(\cos \theta_{0} - \frac{\cos \theta_{1}}{2}\right) \cdot \frac{\theta_{1} - \theta}{\theta_{1} - \theta_{0}}, \quad \theta_{1} < \theta < \theta_{2}$$

$$S^{2}(\theta) = 0 \qquad \qquad \theta \geq \theta_{2} \qquad (C-4)$$

 θ_2 is the angle in which the active element pattern as given by the third equation is zero. A sample calculation has been performed on an antenna array in which the element spacing is 0.7 λ . The measured and the computed patterns are shown in Figure C-1. The agreement is remarkable.

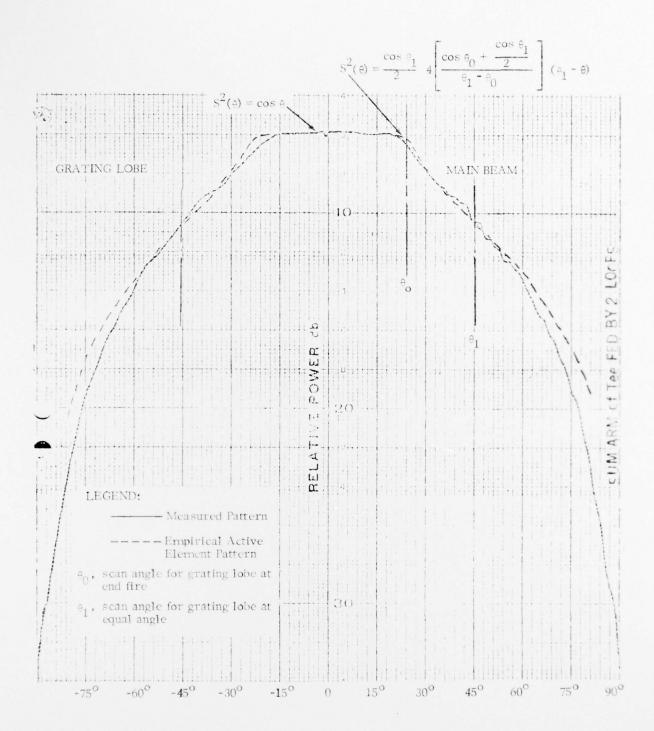
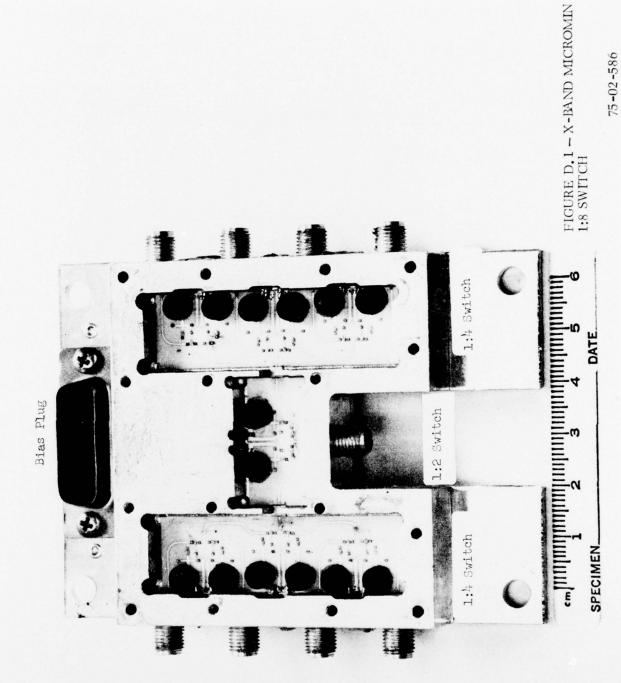


FIGURE C.1 - ACTIVE ELEMENT PATTERN FOR APERTURE FIELD CALCULATION.

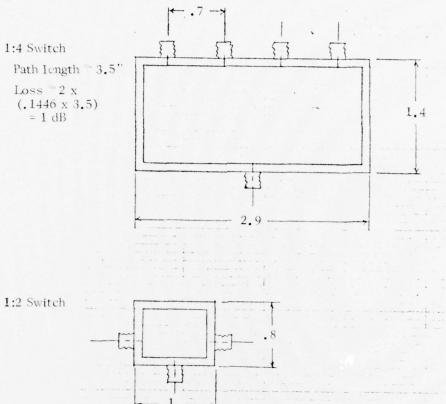
APPENDIX D - BEAM SWITCHING MATRIX LOSSES

The transmission loss through the beam switching matrix has been estimated. The 1:2 and 1:4 X-band micromin switches shown in Figures D.1 and D.2 are assumed to be used as a basic element of the switching matrix. Semiflexible cables (.141µ diameter) are used to interconnect the various switches. Cable lengths are estimated based on the size of the switch units and the clearance required for crisscrossing the cables. Tables D.1 to D.4 show the parts list and the loss tabulation for the cases of 8, 16, 32 and 64 simultaneous beams, respectively. Table D.5 pertains to the case of combining eight 2 x 2 beam clusters to provide eight simultaneous beams.

The estimated losses are rather high based on the mentioned switch design. In order to reduce these losses, more components within the switching trees must be integrated into one single unit. For example, instead of forming a 1:16 tree by connecting five =:4 switches, the 1:16 tree can be built on a single substrate. Furthermore, instead of using .141 inch cables, quarter inch cable, for example, may be used. Then, the line loss would be considerably lower; however, the size of the beam switching matrix must also increase considerably. Even if the low loss components are used, the total loss probably cannot be reduced to a point where RF amplification is not needed.



Design information for X-band switch (micromin) (from Burns and Charlton)



Line loss for 50-line = .07 dB/ λ_d

$$\lambda_{\alpha} = \frac{\lambda_{o}}{\sqrt{\varepsilon_{eff}}}$$
 $\varepsilon_{ff} = 6.6 \text{ for w} = .025 \text{ on .025" alumina}$

at 9.5 GHz, Loss = .07 dB/.4839" = .1446 dB/in.

Rule of Thumb = Multiply the line loss by 2 to account for the diode loss.

FIGURE D.2 - MICROMIN SWITCH DESIGN INFORMATION.

TABLE D.1 - PARTS LIST AND LOSS FOR

| Number of simultaneous beams | = 8 | (s) |
|------------------------------|------|-----|
| Number of groups | = 13 | (m) |
| Number of beams in a group | = 16 | (n) |

| Parts List | Number of Units | Loss per Unit, dB |
|--|-------------------------------|------------------------|
| First Level | | |
| Input cable, length IP4T switch IP2T switch Connecting cable, length | 208, 6" 65 0 52, 7" | .24 1. |
| Second Level | | |
| Input cable, length IP4T switch IP2T switch Connecting cable, length | 13, 35" 26 13 26, 4" | 1.4 1. .3 .16 |
| Third Level | | |
| Input cable, length 1P4T switch 1P2T switch Connecting cables, length | 104, 25" 40 0 32, 7" | .28 |
| Total | | |
| 1P4T switch 1P2T switch SPDT junctions Number of cables Loss | 131 13 406 435 | 6.66 dB |

TABLE D.2 - PARTS LIST AND LOSS FOR

| Number of simultaneous beams | = | 16 | (S) |
|------------------------------|---|----|-----|
| Number of groups | = | 13 | (m) |
| Number of beams in a group | | 16 | (n) |

| Parts List | Number of Units | Loss per Unit, dB | |
|--|-------------------------|-------------------|--|
| First Level | | | |
| Input cable, length 1P4T switch 1P2T switch Connecting cable, length | 208, 6" 80 64, 7" | .24 | |
| Second Level | | | |
| Input cable, length 1P4T switch 1P2T switch Connecting cable, length | 16, 35" 80 64, 7" | 1.4 1. | |
| Third Level | | | |
| Input cable, length 1P4T switch 1P2T switch Connecting cable, length | 256, 30 80 64, 7" | 1.2 1. | |
| Total | 0.1, | .20 | |
| 1P4T switch 1P2T switch | 240 | | |
| SPDT junctions Number of cables | 720 672 | | |
| Loss | | 6.68 dB | |

TABLE D.3 - PARTS LIST AND LOSS FOR

| Number of simultaneous beams | | 32 | (S) |
|------------------------------|---|----|-----|
| Number of groups | = | 32 | (m) |
| Number of beams in a group | = | 7 | (n) |

| Parts List | | Number | of Units | Loss per Unit, dB |
|--|----|----------------------------|----------|---------------------------------------|
| First Level | | | | |
| Input cable, len 1P4T switch 1P2T switch Connecting cabl | | 224, 64 32 64, | | .24 1. .3 .16 |
| Second Level | | | | |
| Input cable, len 1P4T switch 1P2T switch Connecting cabl | | 32, 320 32 320, | | 1,4 2 x 1, (2 levels) .3 .28 |
| Third Level | | | | |
| Input cable, len 1P4T switch 1P2T switch Connecting cabl | | 1024, 320 32 320, | | 2,0 2 x 1, (2 levels) .3 .28 |
| Total | | | | |
| 1P4T switch 1P2T switch SPDT junction Number of cable Loss | 28 | 704 96 2208 1984 | | 10.26 dB |

TABLE D.4 - PARTS LIST AND LOSS FOR

| Number of simultaneous beams | = | 64 | (S) |
|------------------------------|---|----|-----|
| Number of groups | = | 64 | (m) |
| Number of beams in a group | = | 4 | (n) |

| Parts List | Number of Units | Loss per Unit, dB |
|---|--------------------------------------|--|
| First Level | | |
| Input cable, length 1P4T switch 1P2T switch Connecting cable, length | 256, 6" 64 | 1. 24 |
| Second Level | | |
| Input cable, length 1P4T switch 1P2T switch Connecting cable, length | 64, 35" 1280 192 1408, 7" | 1.4 2 x 1. (two levels) 2 x .3 (two levels) .28 |
| Third Level | | |
| Input cable, length 1P4T switch 1P2T switch Connecting cable, length | 4096, 60" 1280 192 1408, 7" | 2.4 2 x 1. (two levels) 2 x .3 (two levels) .28 |
| Total | | |
| 1P4T switch 1P2T switch SPDT junction Number of cables Loss | 2624 384 8256 7232 | 10.8 dB |

TABLE D.5 - PARTS LIST AND LOSS FOR

 $8\ \mathrm{simultaneous}$ beams, each by combining a $4\ \mathrm{beam}$ cluster

| Parts List | | Number | of Units | Loss per Unit, dB | |
|------------|---|-----------------------------|-----------|---|--|
| First | Level | | | | |
| | Input cables, length 1P4T switch 1P2T switch Connecting cable, length | 208, 416 208 416, | 6" 4" | .24 1. .3 .16 | |
| Second | Level | | | | |
| | Input cable, length 1P4T switch 1P2T switch Connecting cable, length | 1664, 480 256 704, | 35" 7" | 1.4 2 x 1. (2 levels) 2 x .3 (2 levels) 3 x .28 (3 levels) | |
| Third | Level | | | | |
| | Input cable, length Power combiner (1:4 feed) | 32 , 8 | 7'' | .28 .2 | |
| Total | | | | | |
| | 1P4T switch 1P2T switch SPDT junction Number of cables Loss | 896 464 3152 3024 | | 7 . 02 dB | |

X. REFERENCES

- 1. R. J. Mailloux, P. R. Caron, J. L. LaRussa, and C. J. Dunne, "Phase Interpolation Circuits for Scanning Phased Arrays," NASA Technical Note No. TN-D-5865, July 1970.
- W. Rotman, "Wide-angle Scanning with Microwave Double-layer Pillboxes," IRE Transactions on Antennas and Propagation, pp. 96-105, January 1958.
- 3. Stein, "Cross Coupling on Multiple Beam Antenna, PGAP, September 1962, pp. 548-557.
- 4. R. Tang and L. Stark, 'High Resolution Hemispherical Reflector Antenna Technique,' Proc. of Symposium on Electrically Scanned Array Techniques and Applications, RADC-TDR-64-255, Vol. II. July 1964, pp. 73-97, (SECRET).
- 5. J. L. McFarland and J. S. Ajioka, "Multiple Beam Constrained Lens," Microwaves, August 1963, pp. 81-89.
- S. Silver, Vol. 12, Rad. Lab Series, page 4, McGraw-Hill Book Co., 1949.
- 7. J. C. Slater, "Microwave Transmission," page 259, Dover Publications, Inc., June 1959.
- 8. P. W. Hannan, "The Element Gain Paradox for a Phased-array Antenna," PGAP, pp. 423-433, July 1964.

METRIC SYSTEM

BASE UNITS:

| BASE UNITS: | | | |
|------------------------------------|---------------------------|-----------|--------------------|
| Quantity | Unit | SI Syr | nbol Formula |
| length | metre | | |
| mass | kilogram | in | |
| time | second | kg | |
| electric current | ampere | s A | |
| thermodynamic temperature | kelvin | K | |
| amount of substance | mole | mol | |
| luminous intensity | candela | cd | |
| SUPPLEMENTARY UNITS: | | | |
| plane angle | radian | | |
| solid angle | steradian | rad sr | |
| DERIVED UNITS: | | 31 | |
| Acceleration | metre per second squared | | |
| activity (of a radioactive source) | disintegration per second | | m/s |
| angular acceleration | radian per second squared | | (disintegration)/s |
| angular velocity | radian per second squared | | rad/s |
| area | square metre | | rad/s |
| density | kilogram per cubic metre | | m |
| electric capacitance | farad | 17 | kg m |
| electrical conductance | siemens | F | A·s/V |
| electric field strength | volt per metre | S | AN |
| electric inductance | henry | | V/m |
| electric potential difference | volt | H | V·s/A |
| electric resistance | ohm | V | W/A |
| electromotive force | volt | V | V/A |
| energy | ioule | | W/A |
| entropy | joule per kelvin | 1 | N-m |
| force | newton | N | J/K |
| frequency | hertz | | kg·m/s |
| illuminance | lux | Hz | (cycle)/s |
| luminance | candela per square metre | lx | lm/m |
| luminous flux | lumen | 1 | cd/m |
| magnetic field strength | ampere per metre | lm | cd-sr |
| magnetic flux | weber | Wb | A/m |
| magnetic flux density | tesla | T | V·s |
| magnetomotive force | ampere | | Wb/m |
| power | watt | A W | |
| pressure | pascal | Pa | l's |
| quantity of electricity | coulomb | C | Nm |
| quantity of heat | ioule | 1 | A·s |
| radiant intensity | watt per steradian | | N-m W/sr |
| specific heat | joule per kilogram-kelvin | | |
| stress | pascal | Pa | J/kg-K |
| thermal conductivity | watt per metre-kelvin | r a | N/m |
| velocity | metre per second | | W/m-K |
| viscosity, dynamic | pascal-second | | m/s |
| viscosity, kinematic | square metre per second | | Pa·s |
| voltage | volt | V | m/s |
| volume | cubic metre | 1 | W/A |
| wavenumber | reciprocal metre | | m |
| work | ioule | 1 | (wave)/m |
| | | | N-m |
| SI DDFFIVEC. | | | |

SI PREFIXES:

| Multiplication Factors | Prefix | SI Symbol |
|-------------------------------------|--------|-----------|
| 1 000 000 000 000 = 1012 | tera | Т |
| $1\ 000\ 000\ 000 = 10^9$ | Kika | G |
| 1 000 000 = 10* | mega | M |
| 1 000 = 103 | kilo | k |
| $100 = 10^{2}$ | hecto* | h |
| 10 = 101 | deka* | da |
| $0.1 = 10^{-1}$ | deci* | d |
| $0.01 = 10^{-1}$ | centi* | C |
| 0.001 = 10-1 | milli | m |
| 0.000 001 = 10. • | micro | μ |
| $0.000\ 000\ 001 = 10^{-4}$ | nano | n |
| $0.000\ 000\ 000\ 001 = 10^{-12}$ | pico | D |
| 0.000 000 000 000 001 = 10-14 | femto | 1 |
| 0.000 000 000 000 000 001 = 10 - 14 | atto | 0 |

^{*} To be avoided where possible

MISSION

Of

Rome Air Development Center

RADC plans and conducts research, exploratory and advanced development programs in command, control, and communications (C³) activities, and in the C³ areas of information sciences and intelligence. The principal technical mission areas are communications, electromagnetic guidance and control, surveillance of ground and aerospace objects, intelligence data collection and handling, information system technology, ionospheric propagation, solid state sciences, microwave physics and electronic reliability, maintainability and compatibility.

Printed by United States Air Force Hanscom AFB, Mass. 01731